An experimental study of unsteady separation in a two-dimensional flow

by

Raul Javier Coral Pinto

B.S. in Aerospace Engineering, Massachusetts Institute of Technology (2003)
B.S. in Mathematics, Massachusetts Institute of Technology (2003)

Submitted to the Department of Mechanical Engineering
in partial fulfillment of the requirements for the degree of

Master of Science in Mechanical Engineering

at the

MASSACHUSETTS INSTITUTE OF TECHNOLOGY

June 2005

Signature of Author .....

Certified by .....

Thomas Peacock
Assistant Professor
Thesis Supervisor

Certified by .....

Accepted by .....

Lallit Anand
Chairman, Committee on Graduate Students
Department of Mechanical Engineering

An experimental study of unsteady separation in a two-dimensional flow

by

Raul Javier Coral Pinto

Submitted to the Department of Mechanical Engineering
on 6 May 2005, in partial fulfillment of the
requirements for the degree of
Master of Science in Mechanical Engineering

Abstract

An experimental study of flow separation in an incompressible two-dimensional unsteady flow was undertaken with the aim of validating recently developed flow separation criteria, which are based on kinematic principles. Specifically, the so-called rotor-oscillator arrangement was utilized to perform a series of experiments in steady, unsteady periodic, and aperiodic two-dimensional viscous flows at low Reynolds number. Flow separation under these conditions was investigated by means of flow visualization, shear stress sensors, and numerical simulation. The existence of fixed and moving separation structures, as predicted by the recent criteria, was verified in the experiments. Fixed separation structures were encountered in periodic flows and random flows, while moving separation was observed in a slow periodic flow and a random flow with linear drift. It was determined that separation in the rotor-oscillator experiment is strongly correlated to two factors: flow unsteadiness and flow ejection from the wall. The balance of the characteristic length and time scales of unsteadiness and ejection determines whether the separating structure is moving or is fixed. The experimental and numerical results strengthen the notion that the instantaneous zero skin friction point alone does not denote flow separation in unsteady flow. Rather, flow separation in unsteady flow can be better understood from a Lagrangian perspective, in which case it can be treated in a robust and coherent manner.

Thesis Supervisor: Thomas Peacock
Title: Assistant Professor

Thesis Supervisor: George Haller
Title: Associate Professor

Contents

List of Figures

List of Tables

Chapter 1

Introduction

The first accepted description of flow departing from a boundary wall was developed by Prandtl [17]. Taking an Eulerian approach, Prandtl demonstrated that flow separation in a steady incompressible two-dimensional flow occurs at the position on the boundary wall where the skin friction vanishes and admits a negative gradient along the wall. The issue of where flow separates from a boundary wall in unsteady flow, however, has been debated by researchers over the last century [21]. Indeed, at present there is no broadly accepted definition of what is implied by unsteady flow separation, and detailed understanding of the underlying mechanisms has yet to be agreed upon.

The criteria developed for steady flows have served as a basis to attempt to describe separation in an unsteady general flow. Both, Eulerian and Lagrangian views of the flow field have been employed [10]. Within the Eulerian perspective Rott [18] and Moore [16] performed theoretical studies, Sears & Telionis [20] made numerical studies of boundary-layer type flow, while Vidal [26] and Ludwig [15] performed experimental work on unsteady boundary layer separation. Subsequently, their observations culminated in a comprehensive review by Sears & Telionis [21], which initiated the notion that the positioning of the zero skin friction point does not denote the location of the separation structure in unsteady flow.

Based upon the body of work presented by Sears & Telionis [21], the Moore-Rott-Sears (MRS) principle was proposed as a criterion for unsteady flow separation. The MRS criterion states that flow separation results from a point singularity off the wall where the shear vanishes and its local velocity is equal to the velocity of the separation structure. Implementation of

these criteria is impractical however, since it requires the knowledge of quantities away from the wall and an a priori knowledge of the speed of the separation structure.

Unsteady separation viewed from a Lagrangian perspective was proposed by Van Dommelen [24] and Van Dommelen & Shen [25]. The authors performed numerical studies of the Prandtl boundary layer equations in Lagrangian coordinates. Their work succeeded in removing previous difficulties that had halted the Eulerian integration of the boundary layer equations, and concluded that separation takes place at a singularity point where the boundary layer solution becomes numerically unstable. Furthermore, they identified separation as a material spike arising from infinite stretching of a fluid particle in the direction normal to the wall and contraction along the wall. Although this work is pivotal in demonstrating the Lagrangian nature of unsteady separation, further analytical work by Liu & Wan [14] refuted the existence of singularities as an indication of boundary layer separation.

In later work following the Lagrangian spirit, Shariff et al. proposed a theory to describe flow separation in incompressible two-dimensional time-periodic flows [22]. Shariff considered separation as a fixed point on the wall that anchors an unstable manifold which exists in the Poincaré map of the periodic flow. This work first showed that separation in a periodic flow occurs at the location where the average over time of the skin friction vanishes. This approach was made more rigorous by Yuster & Hackborn [27] who reformulated the vanishing mean-skin friction criteria for small-amplitude quasi-steady time-periodic incompressible flows. These developments were supported experimentally by Hackborn, Ulucakli &Yuster [8]. The experimental investigations employed a rotor-oscillator flow configuration to study separation, demonstrating that flow separation can be studied at low Re.

Capitalizing on the Lagrangian notions of unsteady flow separation, Haller developed a general criteria to describe flow separation in a two-dimensional compressible unsteady flow [10]. Haller considered two types of separation structures in unsteady flows: moving and fixed separation. The criteria determine separation from quantities on the boundary and corroborate the idea that flow separation is not determined by the instantaneous zero skin friction point, but requires a knowledge of the time history of surface quantities. Experimental verification of the contributions by Haller remains to be performed; this is the aim of the current experimental work.

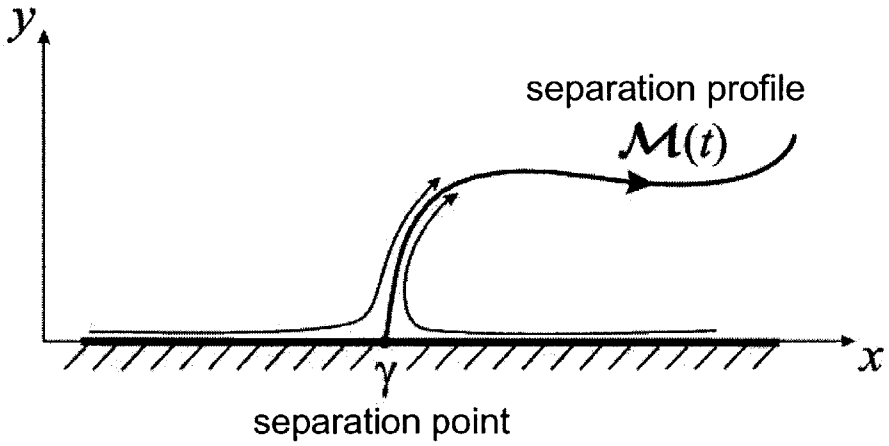

Figure 1-1: Flow separation occurring at the boundary wall. The separation profile makes a finite angle with the wall. Figure taken from Haller [10]

1.1 Theory of two-dimensional unsteady flow separation

An exact theory of unsteady separation for two-dimensional flows has been developed by Haller [10]. The results obtained in this theory are valid for any mass-conserving flow. Separation criteria are derived by considering the existence of a distinguished material line which attracts fluid particles and ejects them away from the boundary. Hence, the distinguished material line takes the name of *separation profile,* $\mathcal{M}(t)$. Anchoring the separation profile to a point on the wall exists a location henceforth defined as the *separation point,* γ. Additionally, in order to guarantee separation there is a finite *separation angle* that the separation profile makes with the boundary wall. These definitions are illustrated in figure 1-1.

1.2 Fixed separation criteria

We begin by considering separation occurring at a fixed position on the boundary. In this type of separation, the location for flow break away from the boundary remains fixed for all times and anchors a time dependent separation profile. In dynamical systems this separation profile is known as an invariant unstable manifold [5]. The separation profile is unique at all times in fixed separation [10].

The unsteady separation criteria derived by Haller are based on three fundamental assumptions: (*i*) there exists only one separation profile emanating from a separation point; (*ii*) the separation profile is not tangent to the boundary wall; (*iii*) the derivatives of the separation profile remain uniformly bounded. These assumptions ensure physical plausibility as well as mathematical rigor of the criteria. Statement (*i*) is automatically satisfied in mass preserving flows without mass sinks or sources. Statement (*ii*) arises from physical observation; fluid at the vicinity of a boundary wall separates when it departs from the surface and therefore does not allow the existence of a tangent separation profile. Finally, statement (*iii*) prevents mathematical unboundedness when deriving the separation formulae.

The criteria give rise to two necessary mathematical conditions for flow separation to occur at a point $\mathbf{p} = (\gamma, 0)$ as illustrated in figure 1-1. The first condition for separation enforces the non-tangency of the separation profile. For this point to exist in a compressible unsteady fluid flow Haller [10] derived the following criterion

$$\boxed{\limsup_{t\to-\infty} \left| \int_{t_0}^{t} \frac{u_y(\gamma,0,\tau)}{\rho(\gamma,0.\tau)} d\tau \right| < \infty.} \tag{1.1}$$

In equation (1.1) u is the horizontal component of the velocity, u_y the rate change of the horizontal velocity in the y direction perpendicular to the boundary, and ρ the wall density. The integral is evaluated in backward time, from the present time t_0 to any past time t. Mathematically, this condition states that a separation point cannot exist if the material line does not posses a finite slope relative to the direction perpendicular to the boundary at all times. The slope of the material line describes the angle of flow separation. This type of separation point is characteristic of flows where there exists a point on the boundary wall where the skin friction has a zero mean for all times. This condition can be met by steady, unsteady periodic or aperiodic flows.

In incompressible periodic flows the separation condition (1.1) reduces to

$$\int_0^T u_y(\gamma, 0, t) dt = 0, \tag{1.2}$$

where T is the period of the oscillatory flow. Here, the relevant time scale that contains all the dynamics of the flow is the period T; any time scale greater than T provides redundant

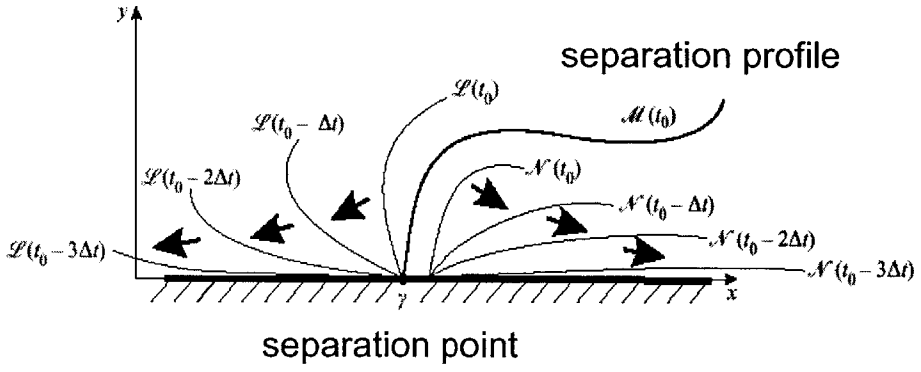

Figure 1-2: The second criterion for flow separation requires that material lines to the left and right of the separation profile align with the wall in backward time. This condition can not be satisfied by a fluid at rest. Figure taken from Haller [1].

information. Equation (1.2) agrees with the results obtained by Shariff et al. [22].

In steady incompressible flows, the density is constant, and the limit of the integral in equation (1.1) remains bounded when the rate of change of u in the y direction vanishes at the separation point. Physically, the quantity u_y can be related to the shear stress τ_w through

$$\tau_w(x,0) = \nu\rho u_y(x,0), \tag{1.3}$$

where ν is the kinematic viscosity. Thus, in steady state condition (1.1) for flow separation is equivalent to Prandtl's first criterion [17]:

$$\tau_w(p) = \nu\rho u_y(p,0) = 0. \tag{1.4}$$

The criterion (1.1) for separation is also satisfied by a flow at rest. In order to ensure there is flow, a second criterion is necessary. The second separation criterion states that there is a unique material line distinguished by the fact that all other material lines converge to the boundary wall in backward time. Figure 1-2 portrays the second criterion. This condition

cannot be satisfied by a fluid at rest, and is expressed mathematically as follows

$$\boxed{\lim_{t\to-\infty}\int_{t_0}^{t}\left[\frac{1}{\rho(\tau)}(u_{xy}(\gamma,0,\tau)-v_{yy}(\gamma,0,\tau))-2v_{xy}(\gamma,0,\tau)\int_{t_0}^{\tau}\frac{u_y(\gamma,0,s)}{\rho(\gamma,0,\tau)}ds\right]d\tau=\infty.} \tag{1.5}$$

In equation (1.5), v is the flow velocity in the y direction, x is the axis along the wall, and the subscripts indicate partial derivatives taken along the x and y directions.

In periodic incompressible flows equation (1.5) reduces to

$$\int_0^T u_{xy}(\gamma,0,t)dt<0. \tag{1.6}$$

Regardless of the flow time dependence, flow separation is observable only if both separation criteria are satisfied; equations (1.1) and (1.5) are considered necessary conditions for flow separation.

For steady incompressible fluids equation (1.5) reduces to Prandtl's second criterion for flow separation.

$$\tau_{wx}(p)=\nu\rho u_{xy}(p,0)<0. \tag{1.7}$$

This criteria can be understood physically as follows: the shear stress of the wall is the signature of the direction and magnitude of the fluid flow passing over the boundary. When separation occurs, the shear stress changes sign to account for different flow directions on each side of the separation point. Thus, the shear stress admits a negative gradient along the wall.

Additionally, the theoretical work developed by Haller permits determining the shape of the separation profile [10]. The equations for the separation profile are obtained using the third fundamental assumption for the theoretical construction: the separation profile is continuously differentiable. The separation profile can then be reconstructed utilizing Taylor expansions. For unsteady incompressible flows the slope of separation, or linear approximation of the separation profile, is written as

$$\boxed{f_0(t_0)=\lim_{t\to-\infty}\frac{\int_{t_0}^{t}\left[u_{yy}(\gamma,0,\tau)+3u_{xy}(\gamma,0,\tau)\int_{t_0}^{\tau}u_y(\gamma,0,s)ds\right]d\tau}{3\int_{t_0}^{t}u_{xy}(\gamma,0,\tau)d\tau},} \tag{1.8}$$

where f_0 is the slope of the separation profile at the current time t_0. In the absence of time de-

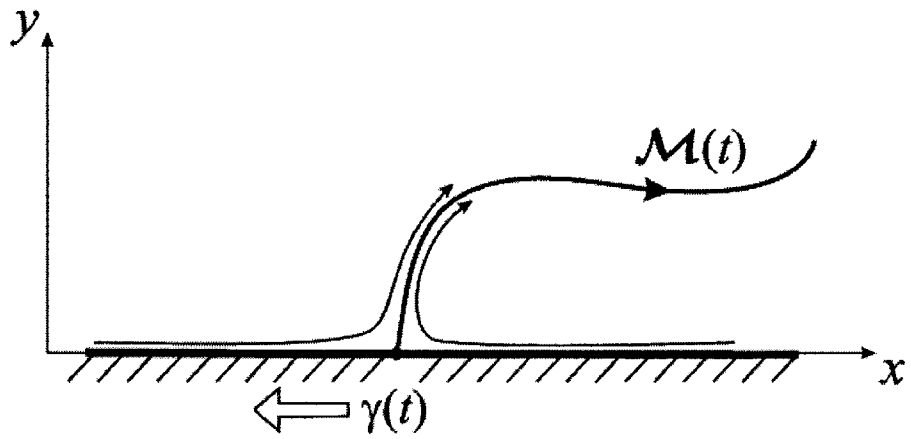

Figure 1-3: Moving separation in unsteady flow, Figure taken from Haller [10].

pendence, equation (1.8) becomes Lighthill's formula for steady incompressible flow separation [13].

1.3 Moving separation criteria

The previous section summarized the theory formulated for a fixed separation point in an unsteady flow. On the other hand, an unsteady flow without a zero mean skin friction point on the boundary can not have a fixed separation point. A separation point that is not stationary and moves along the boundary wall is called a moving separation point. In moving separation, the material line that draws fluid from the boundary has a finite life time. For times exceeding this, the separation point moves and its motion is accompanied by the creation of a new attracting material line anchored at a new separation point. In dynamical systems these material lines are termed as finite-time invariant manifolds [9], and the separation profile they create is non-unique in moving separation [10]. Moving separation is illustrated in figure 1-3

In order to describe moving separation, the lack of a time scale that circumscribes all the dynamics of the fluid requires the formulation of the concept of effective separation point. Haller

defines an effective separation point γ_{eff} as the location in the boundary wall that satisfies

$$\int_{t_0}^{t} \frac{u_y(\gamma_{eff}, 0, \tau)}{\rho(\gamma_{eff}, 0, \tau)} d\tau = 0. \tag{1.9}$$

It is the point of zero mean shear stress for the time interval t_0 to t. In fixed separation the effective separation point is the true separation point. For moving separation, the effective separation point converges to the true separation point as time advances [10]. The location of the moving separation point γ, illustrated in figure 1-3, at a determined time is t_0 is given by

$$\gamma(t_0) = \frac{1}{2}[\gamma_+(t_0 - T_m(t_0), t_0) + \gamma_-(t_0 - T_m(t_0), t_0], \tag{1.10}$$

where

$$\gamma_+(t, t_0) = \sup_{s \in [t, t_0)} \gamma_{eff}(s, t_0), \qquad \gamma_-(t, t_0) = \inf_{s \in [t, t_0)} \gamma_{eff}(s, t_0). \tag{1.11}$$

The effective separation points in equation (1.11) determine the interval

$$\delta(t, t_0) = \gamma_+(t, t_0) - \gamma_-(t, t_0), \tag{1.12}$$

which satisfies

$$\frac{1}{2}\delta(t_0 - T_m(t_0), t_0) \int_{t_0 - T_m(t_0)}^{t_0} \max_{x \in I(t_0 - T_m(t_0), t_0)} |u_{xy}(x, 0, t)| dt = 1, \tag{1.13}$$

$$\max_{x \in I(t_0 - T_m(t_0), t_0)} u_{xy}(x, 0, t) < 0, \qquad t \in [t_0 - T_m(t_0), t_0], \tag{1.14}$$

where T_m represents the lifetime of the material line that induces separation. Haller showed that moving separation profiles are not unique, and the time scale T_m distinguishes the material line that stays in the vicinity of an effective separation point for the longest time [10].

In order to obtain approximations for the moving separation profile, the time scale $T_m(t_0)$ is utilized. The linear approximation for the separation profile is given by the slope

$$\boxed{f_0(t_0) = \frac{\int_{t_0}^{t_0 - T_m(t_0)} \left[u_{yy}(\gamma_{eff}, 0, \tau) + 3u_{xy}(\gamma_{eff}, 0, \tau) \int_{t_0}^{\tau} u_y(\gamma_{eff}, 0, s) ds \right] d\tau}{3 \int_{t_0}^{t_0 - T_m(t_0)} u_{xy}(\gamma_{eff}, 0, \tau) d\tau}.} \tag{1.15}$$

1.4 Unsteady separation from physical quantities

The separation conditions (1.1), (1.5), and (1.8) are a function of purely kinematical quantities. Practical applications, however, require criteria expressed in terms of physically measurable quantities. For unsteady incompressible flows, the separation criteria can be expressed as

$$\lim_{t\to-\infty} \sup \left| \int_{t_0}^{t} \tau_w(\gamma, 0, \tau) d\tau \right| < \infty, \tag{1.16}$$

$$\lim_{t\to-\infty} \int_{t_0}^{t} \tau_{wx}(\gamma, \tau) d\tau = \infty. \tag{1.17}$$

Similarly, the slope can be written

$$f_0(t_0) = -\lim_{t\to-\infty} \frac{\int_{t_0}^{t} \left[p_x(\gamma, 0, \tau) + 3\tau_{wx}(\gamma, 0, \tau) \int_{t_0}^{\tau} \frac{1}{\nu\rho} \tau_w(\gamma, 0, s) ds \right] d\tau}{3 \int_{t_0}^{t} \tau_{wx}(\gamma, 0, \tau) d\tau}, \tag{1.18}$$

where p is the pressure. The above equations are derived enforcing the non-slip boundary condition at the wall and using identities resulting from manipulation of the Navier-Stokes equations. These criteria can be utilized for moving and fixed separation after proper manipulation of the time scales for integration.

The above expressions indicate that unsteady flow separation can be resolved by using sensing devices for pressure and shear stress along the boundary wall. Experimentally, it suffices to place an array of sensors near the region of interest to determine flow separation in real time. The criteria developed by Haller are practical, and in principle can be implemented in engineering applications.

1.5 Preview of chapters

The body of this thesis is devoted to validating the main results of the theoretical work developed by Haller [10]. This comprises verifying the existence of fixed separation points, moving separation points, and determining flow separation based on shear stress measurements on the wall.

A description of the theory covering the rotor-oscillator flow is presented in Chapter 2.

Important features of the flow such as its low Reynolds (Re) and Strouhal (Sr) numbers, and description of the relevant analysis and numerics are discussed. Chapter 3 provides a description of the experimental apparatus used to produce a rotor-oscillator flow. The characteristics of the different actuators, data acquisition system, dye visualization, and shear stress sensors are covered.

Experimental and supporting numerical results on flow separation in steady and unsteady flows are treated in Chapter 4, 5, and 6. Chapter 4 considers steady separation in the rotor-oscillator, flow previously studied by Hackborn [8]. Fixed separation points in the unsteady rotor-oscillator flow appear in Chapter 5. Specifically, the existence of a fixed separation point in a periodic flow and a random flow is investigated. Chapter 6 explores moving separation points under two types of unsteady conditions: slow periodic flow and random flow with linear drift. The former results from a rotor oscillation with frequency approaching to zero, while superimposing a random motion with a constant velocity translation produces the latter motion type.

Chapter 7 summarizes the findings of the experiments and comments on the performance of the flow separation criteria. Additionally, this section discusses aspects of the experimental studies that can be further improved for future work.

Chapter 2

The Rotor-Oscillator Flow

The aim of this work is to determine the behavior of an unsteady two-dimensional flow separating from a boundary wall utilizing the separation criteria developed by Haller [10]. To formulate accurate descriptions of unsteady flow separation it is necessary to work with a system that provides: repeatability, observability, and control over the factors that induce the separation. These functional requirements pose challenges because of the varying time and length scales inherent to unsteady flows.

Classical experimental arrangements that might be considered are a forward/backward step flow, and flow over an airfoil. These flow configurations are illustrated in figures 2-1 and 2-2. Both arrangements present a practical engineering application for the separation criteria. However, both require a large apparatus and unsteady separation occurs on short time and length scales that are difficult to visualize and simulate.

We shall consider unsteady separation generated by a so-called rotor-oscillator arrangement. This arrangement was first considered by Hackborn to study flow mixing and separation in Stokes flow [8]. The experimental arrangement consisted of a rotating cylinder immersed in a tank whose sidewall was able to oscillate to introduce unsteadiness to the flow. The resulting flow was two-dimensional. Figure 2-3 indicates a cross section of the flow arrangement considered by Hackborn. Hackborn's experimental and theoretical work shows that flow separation in this configuration is controlled by the rotational speed of the rotor and the oscillatory motion of the sidewall. Furthermore, it was demonstrated that in this arrangement unsteady flow separation occurs on time scales of the order of seconds and length scales of the order of

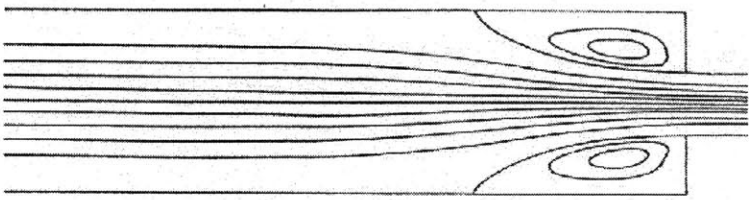

Figure 2-1: Streamlines for flow through sudden expansion in a step flow, Re = 25. Figure taken from Fearn & Mullin [3]. Flow separation occurs on the top and bottom wall of channel.

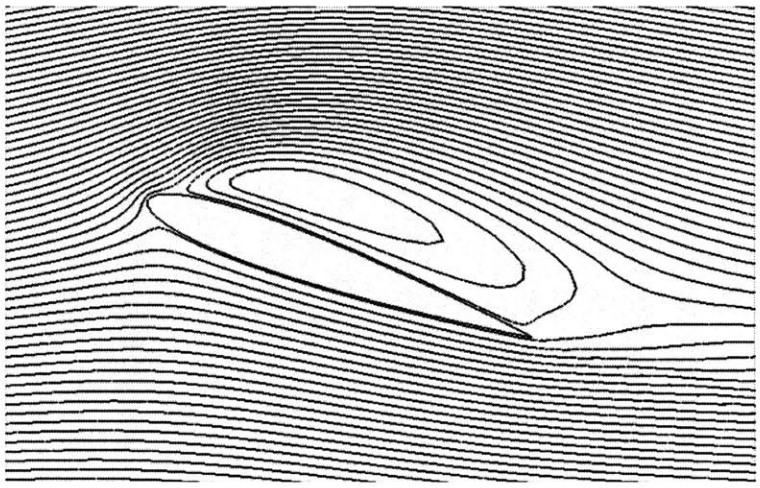

Figure 2-2: Streamlines on NACA0012 airfoil at 19.43 degrees, Ma = 0.3. Figure taken from Sahin [13]. Separation occurs at the leading edge.

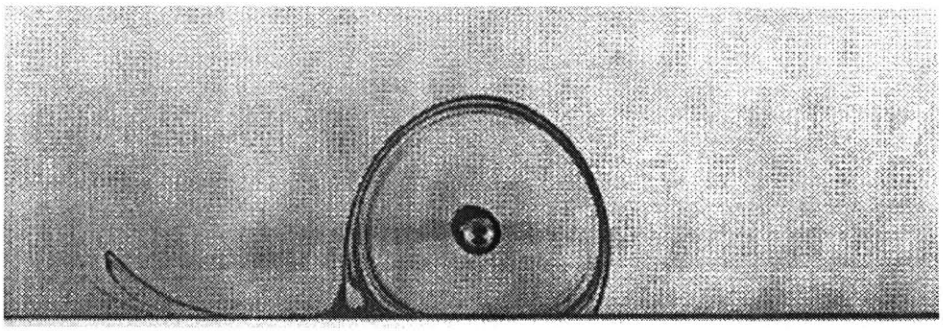

Figure 2-3: Cross section of rotor-oscillator flow arrangement considered by Hackborn [4]. Flow separation and re-attachment occur at the bottom sidewall. The cylinder rotating near the wall is 6 mm in diameter, the flow has Re$\leq$1.

centimeters, making it suitable for experimental investigation.

The experimental construction utilized in the present study, described in detail in chapter 3, consists of a cylinder with rotational motion about its axis and translational motion along the axis of a long fluid tank as indicated in figure 2-4. The latter feature differs from the arrangement proposed by Hackborn, in which it was the sidewall that moved, and allows more flexibility and control over the type of unsteadiness introduced into the flow. The cylinder extends from the top to the bottom of the fluid tank, and the sidewalls of the tank are parallel to the translational motion of the cylinder. Similar to the configuration considered by Hackborn, flow generated by this arrangement is expected to be nominally two-dimensional [8]. Unsteady flow separation occurs at the stationary sidewall. A cross-section of the expected flow is shown in figure 2-5. The location of separation is determined by the type of motion featured by the rotation and translation of the cylinder.

2.1 Governing equations and relevant parameters

Assuming a two-dimensional flow, the governing equations of fluid motion in the experimental configuration are the two dimensional Navier-Stokes equations.

$$\frac{\partial \overline{u}}{\partial \overline{t}} + \overline{u}\frac{\partial \overline{u}}{\partial \overline{x}} + \overline{v}\frac{\partial \overline{u}}{\partial \overline{y}} = -\frac{1}{\rho}\frac{\partial \overline{p}}{\partial \overline{x}} + \nu\left(\frac{\partial^2 \overline{u}}{\partial \overline{x}^2} + \frac{\partial^2 \overline{u}}{\partial \overline{y}^2}\right), \tag{2.1}$$

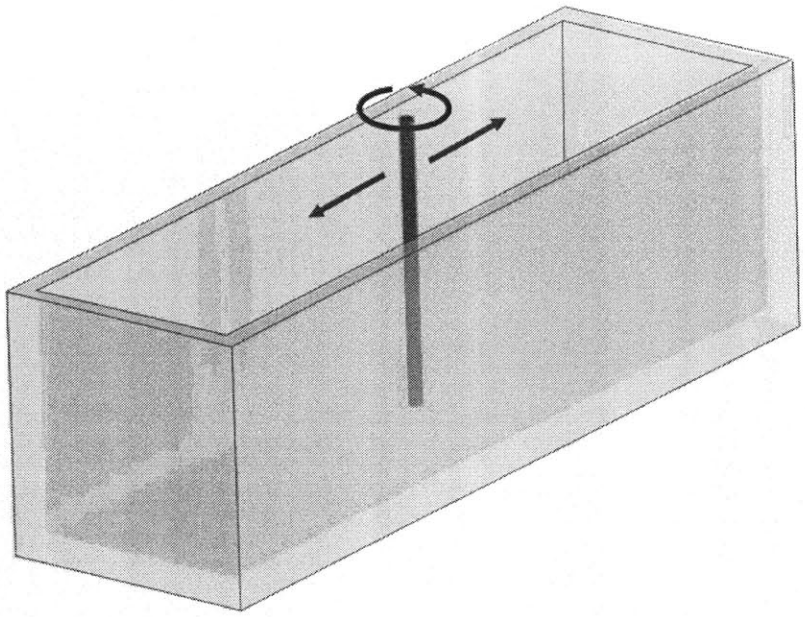

Figure 2-4: Rotor-oscillator configuration. The cylinder rotates around its axis and translates parallel to the sidewalls.

$$\frac{\partial \overline{v}}{\partial \overline{t}} + \overline{u}\frac{\partial \overline{v}}{\partial \overline{x}} + \overline{v}\frac{\partial \overline{v}}{\partial \overline{y}} = -\frac{1}{\rho}\frac{\partial \overline{p}}{\partial \overline{y}} + \nu\left(\frac{\partial^2 \overline{v}}{\partial \overline{x}^2} + \frac{\partial^2 \overline{v}}{\partial \overline{y}^2}\right), \tag{2.2}$$

where $\overline{u}$ is the velocity in the x direction, $\overline{v}$ is the velocity in the y direction, and $\overline{p}$ is the pressure. The high viscosity of the fluid employed in the experiments permits the simplification of the inertial terms yielding the Stokes equations. This standard procedure is performed by means of non-dimensionalization, using the relevant physical parameters that control the dynamics of the experiment.

The driving mechanism of motion in the fluid is the cylindrical rotor. The rotor has a characteristic radius r, and is rotating at angular velocity ω. The momentum provided by the rotating cylinder diffuses away towards the walls of the tank. As the tank becomes wider, the velocity of the fluid near the walls decreases; thus an appropriate length scale is the half width of the tank h. In addition to the rotation, the rotor is forced to move back and forth in the direction parallel to the walls with a sinusoidal velocity of characteristic frequency α. Utilizing

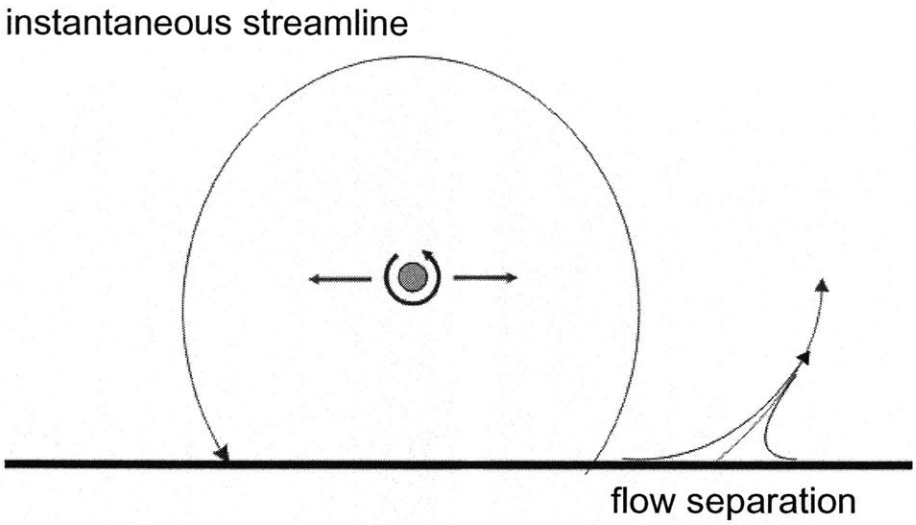

Figure 2-5: Rotor-oscillator cross section for the arrangement in which the cylinder oscillates from side to side. The flow is two-dimensional and separation occurs on the sidewall. The zero shear stress instantaneous streamline is drawn; it makes a revolution around the cylinder.

these parameters a characteristic velocity, steady time scale, and oscillatory time scale can be defined.

In order to define the characteristic velocity it is necessary to consider the radius of the cylinder, r, and the half width of the tank, h. Increasing the size of the rotor results in higher fluid velocity at the tank walls; on the other hand, placing the side walls far apart from the rotor produces slower fluid velocities at the tank boundaries. Thus, the characteristic velocity depends on the tangential velocity of the rotor, ωr, and the ratio of the cylinder radius and the half width of the tank. An appropriate velocity scale is therefore

$$v = \frac{r^2\omega}{h}. \tag{2.3}$$

The steady time scale is obtained from the characteristic length scale, h, and velocity, v, and is given by

$$t = \frac{h^2}{r^2\omega}. \tag{2.4a}$$

The oscillatory time scale is determined by the period of the sinusoidal motion of the rotor,

$$\tilde{t} = \frac{2\pi}{\alpha}. \tag{2.4b}$$

The characteristic parameters in equations (2.3), (2.4a), and (2.4b) define the dimensionless numbers that are relevant to this problem. The Reynolds number

$$Re = \frac{VL}{\nu} = \frac{r^2\omega}{\nu} \tag{2.5}$$

shows the relation of the viscous forces and inertial forces. In order to quantify the importance of the unsteady effects in the fluid, the Strouhal number, Sr, is defined as

$$Sr = \frac{\text{convective time scale}}{\text{forcing time scale}} = \frac{h^2\alpha}{2\pi r^2\omega}. \tag{2.6}$$

Utilizing the characteristic parameters the governing equations can be expressed in dimensionless form with the following substitutions:

$$\left\{\overline{x} = hx, (\overline{u}, \overline{v}) = \frac{a^2\omega}{h}(u, v), \overline{t} = \frac{2\pi}{\alpha}t, \overline{p} \approx \frac{\mu U}{L} = \frac{\mu a^2\omega}{h^2}p\right\}. \tag{2.7}$$

In the cases where the rotor-oscillator experiments have a Re less than unity, it is appropriate to assume that the pressure varies linearly with the characteristic velocity [1]. After substitution into equations (2.1) and (2.2) the dimensionless equations are

$$SrRe\frac{\partial \mathbf{u}}{\partial t} + Re(\mathbf{u} \cdot \boldsymbol{\nabla}\mathbf{u}) = -\boldsymbol{\nabla}p + \boldsymbol{\nabla}^2\mathbf{u}, \tag{2.8}$$

where

$$\mathbf{u} = (u, v). \tag{2.9}$$

In the limit where both Re $\ll 1$ and Sr $\sim O(1)$ the inertial terms can be neglected in equation (2.8) . These forces still exist in the system but are negligible compared to the viscous forces. The fact that the time derivative in the equations can be neglected means the flow can be approximated as quasi-steady. The resulting equations that describe the fluid motion are given

by

$$\nabla^2 \mathbf{u} = \nabla p, \tag{2.10}$$

$$\nabla \cdot \mathbf{u} = \mathbf{0}. \tag{2.11}$$

Equation (2.10) is the vector form of the Stokes equations, while equation (2.11) is the continuity equation for an incompressible fluid. The reduction of the Navier-Stokes equations to the Stokes equations greatly simplifies the mathematical problem. The Stokes equations are linear, thus the superposition principle of solutions can be applied. In addition, the flow has a quasi-steady behavior, namely, the flow time dependence can enter only through the boundary conditions of the problem.

2.2 Steady solution for the rotor-oscillator experiment

Hackborn analyzed the steady flow field resulting from a rotating cylinder immersed in a fluid container of idealized infinitely long walls [6] [7], and validated his mathematical model in a series of experiments that describe separation and mixing regions in a Stokes flow [8]. This section summarizes the steady flow solution for the cylindrical rotor experiments proposed by Hackborn [6].

Due to the high viscosity of the fluid and the geometry of the experiment, the experiment can be modeled as a two-dimensional system laying in the Stokes flow regime. The tank is idealized as two infinitely long plates, due to its relatively large length-to-width ratio (5:1), and the effects of the bottom, end, and surface of the tank are neglected. These assumptions are supported by observations made by Hackborn [8] and Swanson & Ottino [23]. Hackborn observed no effect correlated with the depth and surface of the tank when flow visualization dye was injected far away from both the surface and the bottom. Due to the slowness of the flow at the end walls of the tank, the effect of the ends on the flow field was encountered to be negligible. Hence, the physics of the fluid flow encountered in the experimental setup can be modeled in a two dimensional space.

In order to model the rotational motion of the cylinder, Hackborn utilized a two-dimensional steady line rotlet. A line rotlet is a singularity that exerts a finite torque per unit length on the

surrounding fluid. Mathematically, the line rotlet is commonly written as a stream function of the form

$$\Psi = \sigma \ln(r), \tag{2.12}$$

where σ is the line rotlet strength, and r is the distance from the rotlet origin. It can be readily shown that the torque per unit length exerted by the rotlet is $4\pi\sigma\mu$ [6]. For a stream function to solve the Stokes equations it must be bi-harmonic, specifically, it must satisfy the equation

$$\nabla^4 \Psi = 0. \tag{2.13}$$

The steady line rotlet satisfies this equation and thus satisfies the Stokes equations.

Introducing appropriate Cartesian coordinates and boundary conditions along with the rotlet stream function, Hackborn obtained a closed solution for the steady rotor-oscillator problem. For convenience, dimensionless coordinate axes are imposed on the experiment configuration as shown in figure 2-6. The dimensionless coordinates are obtained from the substitutions

$$\left\{(\overline{x}, \overline{y}) = h(x, y), \overline{c} = hc, \overline{\Psi} = a^2 \omega \Psi\right\}. \tag{2.14}$$

The *y-axis* is located equidistant and parallel to the infinitely long walls, the plates are located at $x = -1$ and $x = 1$, and the rotor is placed at the point $(x, y) = (c, 0)$, where c is the dimensionless distance in the x direction of the rotor from the origin.

The dimensionless stream function solution for the steady rotor problem can be written

$$\Psi = \ln(R_o) + \tilde{\Psi}, \tag{2.15}$$

where R_o is the distance of a point in the flow plane to the cylinder. The first term in (2.15) represents the line rotlet, and the second term, $\tilde{\Psi}$, is the stream function of the undisturbed flow field. In the Cartesian coordinates the line rotlet is written explicitly as

$$\ln(R_o) = \ln\left\{\left[(x-c)^2 + y^2\right]^{1/2}\right\}. \tag{2.16}$$

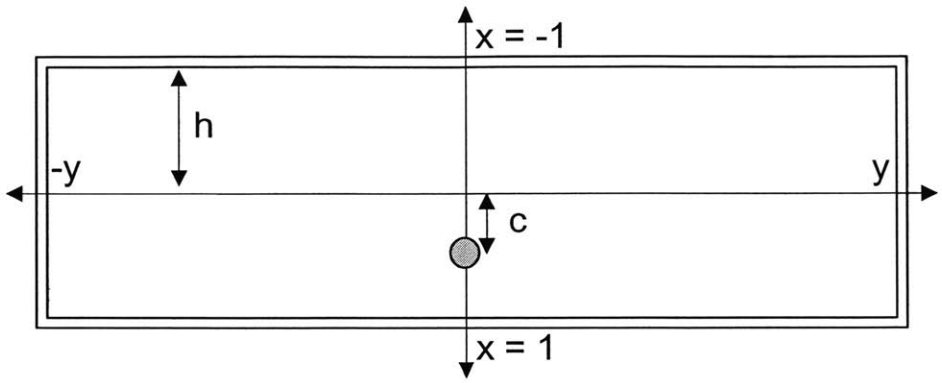

Figure 2-6: Coordinate system for Hackborn's analytic solution of the rotor-oscillator flow.

The velocities in the x and y directions are given by

$$u = -\frac{\partial \Psi}{\partial y}, v = \frac{\partial \Psi}{\partial x}, \tag{2.17}$$

and the boundary conditions are represented by the equations

$$\Psi = \frac{\partial \Psi}{\partial x} = 0, x = \pm 1, \tag{2.18}$$

$$u \to 0, v \to 0, \text{ as } |y| \to \infty. \tag{2.19}$$

Equation (2.18) is the non-slip boundary condition at the walls, and Equation (2.19) bounds the velocity as the walls of the tank extend to infinity. Hackborn showed that the stream function solution that satisfies the above conditions is

$$\Psi = \frac{1}{2} \ln \left\{ \frac{1 - 2e^{1/2\pi y} \cos[1/2\pi(x-c)] + e^{\pi y}}{1 + 2e^{1/2\pi y} \cos[1/2\pi(x+c)] + e^{\pi y}} \right\} + \int_0^\infty h(x,k) \cos(ky) dk, \tag{2.20}$$

where the function $h(x,k)$ is defined to be

$$h(x,k) = 2\frac{[\tanh k \cosh(kx) - x \sinh(kx)] \cosh(kc)}{\sinh(2k) + 2k} + 2\frac{[\coth k \sinh(kx) - x \cosh(kx)] \sinh(kc)}{\sinh(2k) - 2k}. \tag{2.21}$$

Equations (2.20) and (2.21) solve the two-dimensional problem of a rotating cylinder im-

mersed in a tank of infinitely long walls. The solution models the steady case of the rotational cylinder without oscillatory motion in the y direction. For this purpose, a line rotlet singularity has been employed; the rotlet can be seen as a cylinder of infinitesimal radius. The Hackborn solution is valid for $Re < 1$ and Sr of $O(1)$. More details on this solution will be given in chapter 4. Moreover, this steady solution will form the basis of our investigation of unsteady flows in chapter 5 and 6.

Chapter 3

Experimental and numerical methods

In this chapter we describe the apparatus utilized to produce a two-dimensional rotor-oscillator flow, the visualization method to evidence flow separation, and the sensors employed to take shear stress measurements at the wall. Additionally the numerical methods are described. These include a FLUENT model, Gaussian quadrature for integration, and particle tracking.

3.1 Rotor-oscillator physical apparatus

The experimental arrangement comprised a fluid tank, an aluminum structural support, and motion control hardware. An image of the arrangement is shown in figure 3-1. An acrylic tank with dimensions of 12 cm in width, 13 cm in height and 42 cm in length was utilized to contain the fluid. Pressure forces acting on the walls were not a concern because of the small volume of fluid and the walls' thickness of 1 cm. The tank had an open top allowing the fluid to have a free surface exposed to the environment. Fluid was removed from the container by means of a valve located at the base of one of the sidewalls. Supporting the acrylic tank there was an aluminum structure designed to elevate the container 20 cm from ground level. The aluminum structure was firmly fixed to the tank and allowed visualization of the inside fluid from all directions. In order to observe the tank's cross section, a 45 degree mirror was placed underneath the aluminum structure. With the purpose of driving the fluid motion, a cylinder

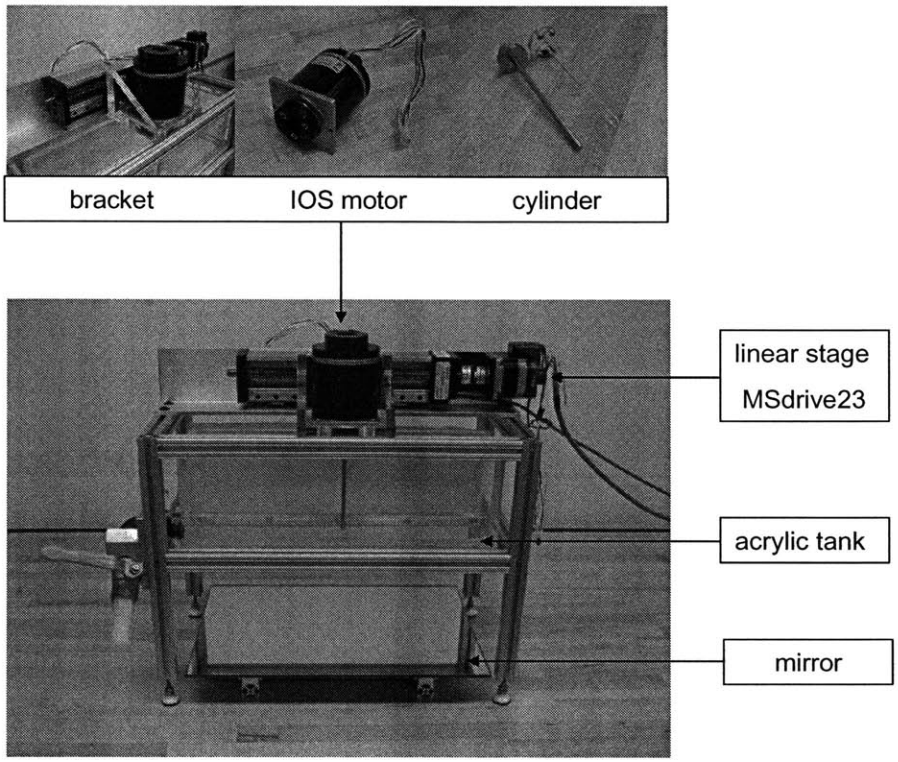

Figure 3-1: Experimental arrangement for rotor-oscillator flow. The picture shows the acrylic tank, aluminum structural support, and motion control hardware.

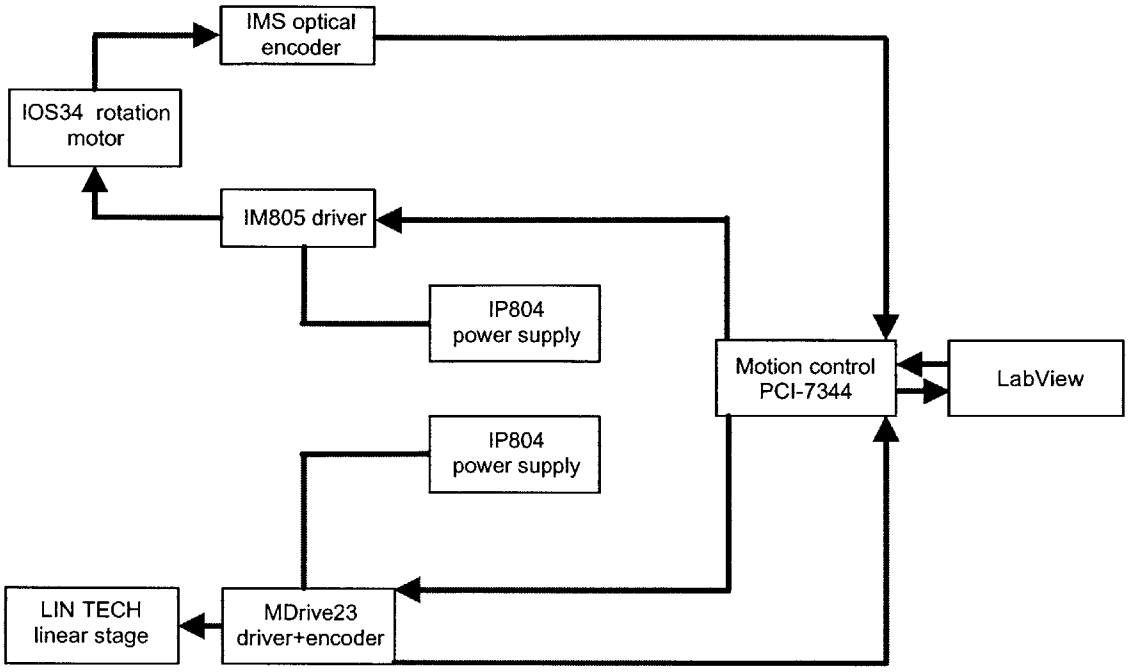

Figure 3-2: Motion control schematic. The upper branch involving the IOS34 motor controlled the rotational motion, while the lower branch involving the MDrive23 controlled the translational motion.

was mounted on a linear stage and immersed into the fluid tank. The cylinder was 12 cm in length and 6 mm in diameter. During the experiments, both an aluminum cylinder and an acrylic cylinder were employed.

A schematic of the motion control in the experiments is presented in figure 3-2. The cylinder possessed two degrees of freedom: rotation around its own axes, and translation along the long axis of the tank. Both motions were controlled using the commercial software LabVIEW version 7 and a motion control card type PCI-7344 from National Instruments. The motors, encoders, stepping drivers, and power supplies were all acquired from Intelligent Motion Systems (IMS). The rotational motion was introduced using an inside-out stepper motor type IOS34 and monitored by an IMS optical encoder with a single end encoder connection. Figure 3-1 shows the IOS motor with the optical encoder incorporated. In order to rotate at the desired angular speed, the motion card PCI-7344 sent orders to a micro-stepping driver type IM805. The translational motion was achieved using a LINTECH linear stage 10" in length. The motion

was driven by a 1/4" lead screw whose rotation translated the IOS motor along the long axis of the tank. The stage motion was driven and monitored by a MDrive23 motor driver that possessed micro-stepping and motion control. In order to power both motors, two unregulated linear power supplies of type IP804 were utilized.

3.1.1 Geometric alignment for rotor-oscillator apparatus

In order to generate a two-dimensional flow it was important to align the experiment components properly. There were three important aspects of the arrangement that needed to be aligned with accuracy: the acrylic tank, linear stage, and cylinder. The acrylic tank was supported by the aluminum structure, as shown in figure 3-1. The horizontal level was set by means of four adjustable screw mounts positioned in the bottom of each leg of the structure. The angle of inclination of the tank relative to the horizontal plane was ± 0.1 degree as measured using a Starett level model #98. The sidewalls of the fluid tank were vertical within ± 1 degrees relative to the direction of gravity as measured with a Dasco Pro angle finder.

Parallel alignment of the stage to the sidewalls was required for translational motion of the cylinder parallel to the long axis of the tank. Alignment was achieved by measuring the distance of the cylinder from the sidewall at different positions along the tank using aluminum gauges accurate within ± 0.1 mm. The procedure consisted of moving the stepper motor to both ends of the linear stage and then measuring the distance of the cylinder from the wall using the aluminum gauges. As a result, the linear stage was aligned to the fluid tank base within ± 0.1 degrees as measured with the Starett level and parallel to the sidewalls of the tank within ± 2 degrees as measured with the Dasco Pro angle finder.

In addition to the parallel translation of the cylinder, it was necessary to have a cylinder whose axis of rotation is perpendicular to the base of the tank. This is important since failing in this requirement results in an eccentric rotational motion. The quality of this alignment depended on the machining quality of the cylinder and the ISO motor. By utilizing micro-positioning, it was determined that the cylinder is straight within 1 mm of its rotational axis.

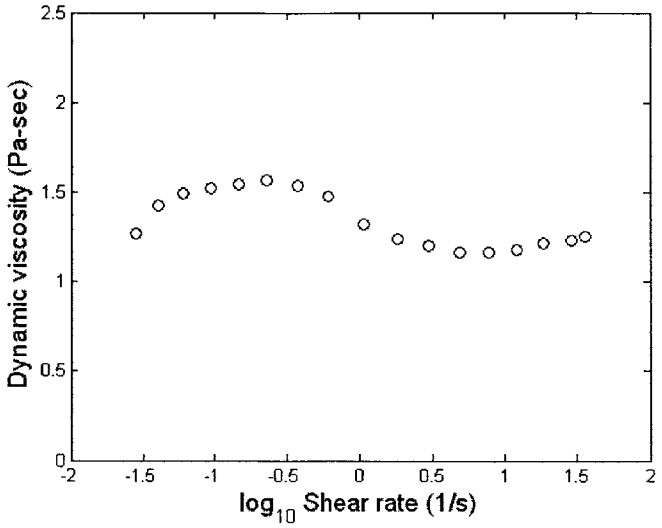

Figure 3-3: Dynamic viscosity of corn syrup-water mixture at T = 20 C. Viscosity mean value is 1.33 Pa-sec.

3.1.2 Viscous fluid for experiments

In order to maintain a small Re viscous fluids were used in the experiments. The experiments to visualize the fluid separation were first run utilizing a corn syrup-water mixture, and glycerol. The preparation of the former fluid consisted of 110 mL of water every 1000 mL of syrup. Using this composition a viscosity close to that of pure glycerol is achieved. In order to confirm that the corn syrup mixture was indeed a Newtonian fluid, the viscosity was measured as function of the shear rate employing a AR1000 rheometer. In figure 3-3 the dynamic viscosity of the corn syrup-water mixture at different shear rates is presented.In general, the results indicated a 7 % standard deviation from the mean viscosity value and therefore the corn syrup mixture was considered a suitable Newtonian fluid for experimentation.

The experiments to acquire shear stress measurements were performed utilizing glycerol. This fluid was also characterized utilizing the AR1000 rheometer. In figure 3-4 the dynamic viscosity of glycerol at different shear rates is presented. In general, glycerol displayed a 3 % standard deviation from the mean viscosity value. The dynamic viscosity of the fluids when performing separation experiments ranged between 1.1 Pa-sec and 1.6 Pa-sec.

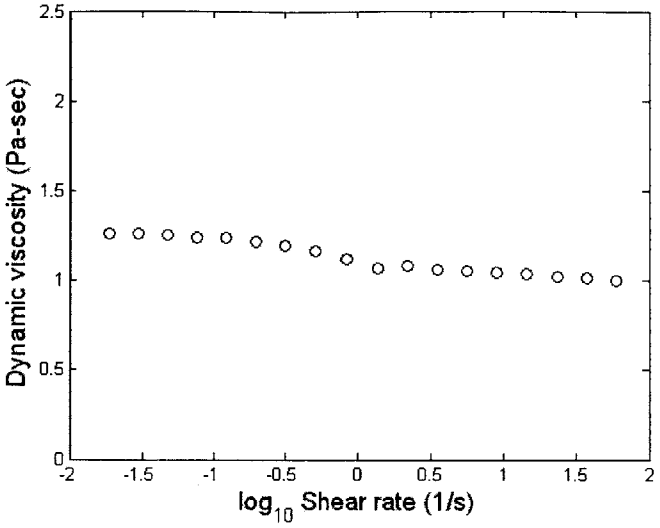

Figure 3-4: Dynamic viscosity of glycerol at T = 20 C. The mean viscosity value is 1.13 Pa-sec.

3.1.3 Flow visualization method

The method for visualization involved placing dye by mechanical means into the fluid flow of the tank. A mixture of fluid and india ink black powder was utilized. By mixing 10 gr of powder dye with 50 mL of the fluid (i.e. corn syrup or glycerol), the dye acquires a fluid form of density similar to the fluid density, thus minimizing buoyancy effects. The dye is placed my means of a syringe with a cylindrical needle 1 mm in diameter. A mechanical stage attached to the aluminum support structure held the syringe. By driving the mechanical stage, the syringe in a typical experiment deposited 3 to 5 cm material lines of dye along the wall before the cylinder started to drive the fluid motion. Additionally, streak line visualizations were performed. This was achieved by attaching a plastic pipe to the wall and drilling holes at different locations along the pipe. The visualizations are presented in the experimental results section.

3.2 Sensor system for shear stress measurements

The hot-wire anemometer system comprised two main subsystems: the hot-wire sensor and the anemometer electronics. The hot-wire sensor was a thin wire made of aluminum. The

anemometer circuit was designed to maintain the hot-wire at constant temperature under flow conditions, requiring bridge balancing of the hot-wire, signal output selection, and hot-wire time response modulation. The anemometer provided a voltage signal related to the shear-stress that could be processed through data acquisition software in a computer platform. The following sections describe the procedures and underlying fundamentals to utilize the hot-wire system developed by Kenny Breuer and his research laboratory at Brown University.

3.2.1 Constant temperature operating principle

Anemometers that operate under constant temperature require a controlled current supply to regulate the heat losses from the sensing element. The heat loss is compensated and a nearly constant resistance sensing element can be achieved. Figure 3-5 shows a schematic of the circuit, in which R is the hot-wire resistance, V_1 is the voltage across the hot wire, and V_0 is the output voltage which is recorded by the anemometer [2]. The constant temperature anemometer circuitry is characterized by a differential DC amplifier, sensing element, and reference voltage. The sensing element is placed in a leg of a Wheatstone bridge, in which feedback is used to maintain the resistance of the hot-wire.

3.2.2 The sensing element

The sensing element was made of a Platinum wire soldered between two electrodes on a PCB board. Figure 3-6 shows a sensor utilized to measure shear stress. Because of its small diameter, 15 μm, the platinum wire is initially coated with zinc, and is commonly known as a Wollaston wire. In order to remove the zinc it was necessary to utilize nitric acid in a 50 % water solution. The Wollaston wire was submerged in the nitric acid for 2 minutes and 30 seconds, the zinc etched and the platinum wire remained. Then, the wire was soldered on the electrodes utilizing a micro-positioner and mildly activated resin flux. The length of the wire was 1.5 mm resulting in a typical resistance of the wire between 9 and 15 Ω.

The sensor in the experiments was part of a 10 sensor PCB board, such as that shown in figure 3-7. The board comprises two rows of 5 sensors each and allows more than one sensor at the time to take measurements. The sensors in the same row have a separation of 4 mm and the two rows are offset by 2 mm. The resulting resolution of the whole board is of 2 mm.

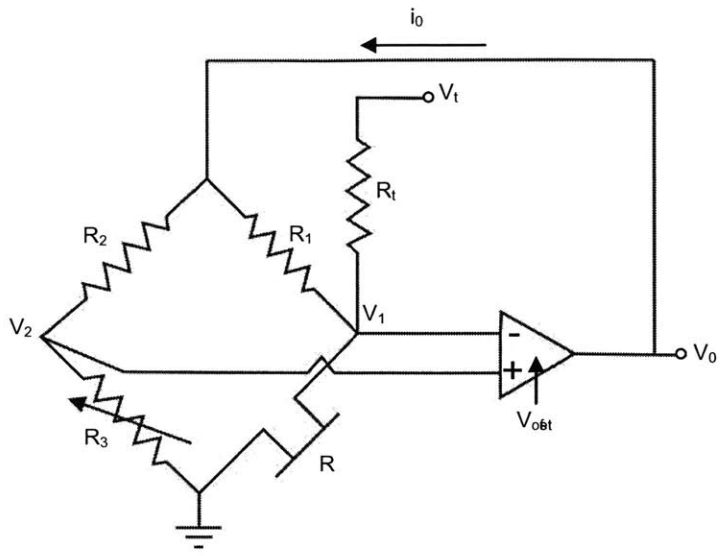

Figure 3-5: Wheatstone bridge circuit for anemometer.

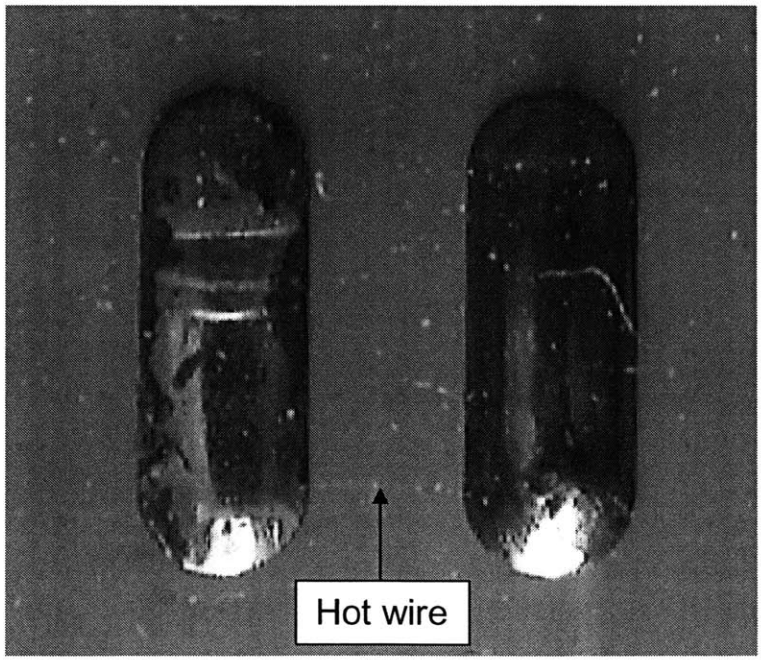

Figure 3-6: Platinum wire soldered between electrodes on PCB board. The electrodes have a length of 3 mm. The wire has a diameter of 15 μm and a length of 1.5 mm.

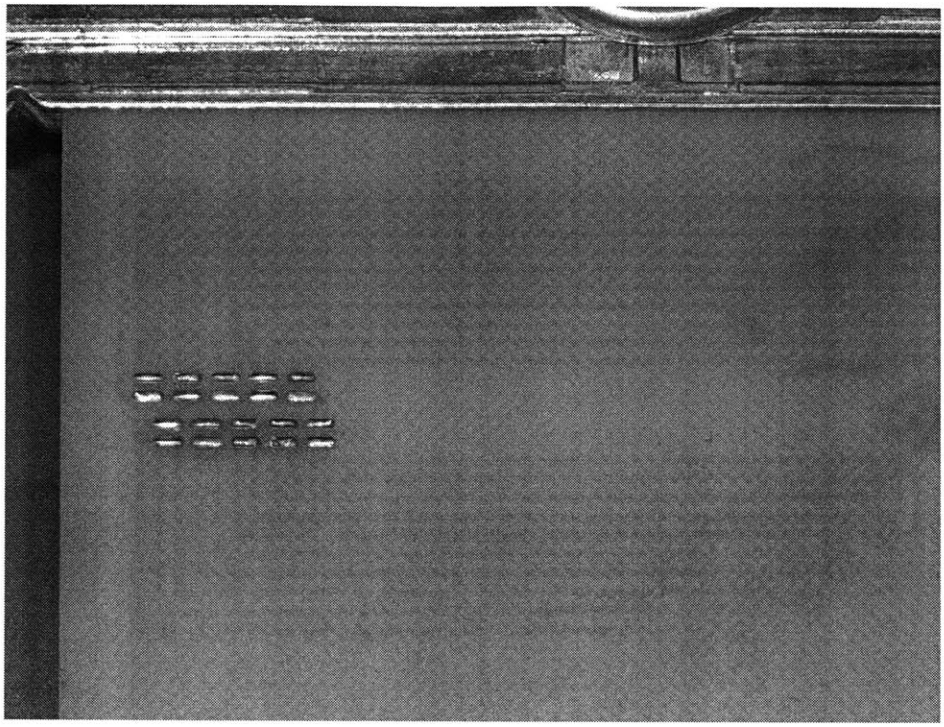

Figure 3-7: Sensor array to take shear measurements.

3.2.3 The Anemometer

The anemometer board controlled the temperature, and thus resistance, of the sensing element. Figure 3-8 indicates the main components of the anemometer. In order to achieve bridge balancing, the resistance R_3, shown in figure 3-5, must be tuned in the anemometer circuit by utilizing the resistance rotary switches. There are four resistance switches rated as follows: coarse, medium, fine, and extra-fine (from left to right as indicated in figure 3-8). They were systematically adjusted to balance the Wheatstone bridge.

Another important parameter is the overheat ratio, which is defined as

$$a_T = \frac{T - T_0}{T_0}, \tag{3.1}$$

where T_0 is the ambient reference temperature, and T is the temperature of the sensing element.

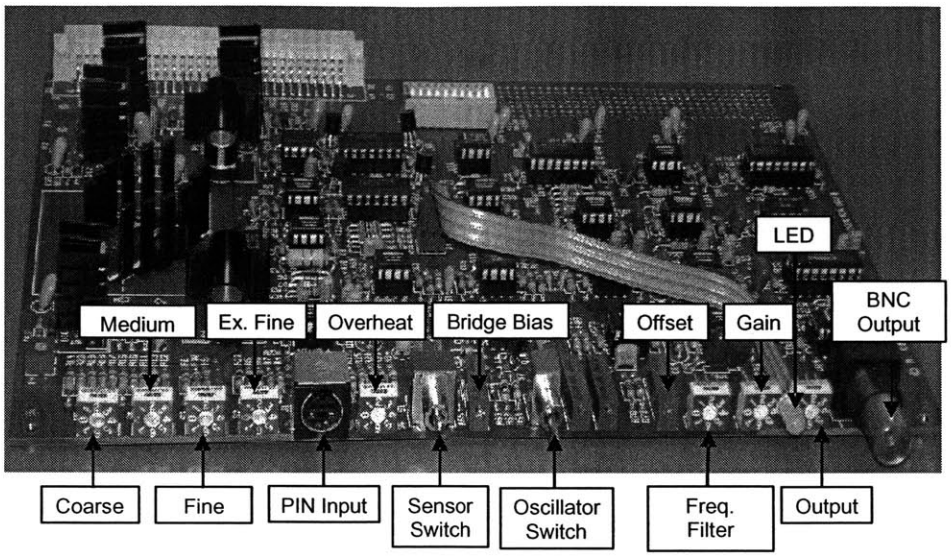

Figure 3-8: Anemometer board and its components.

In practice, the resistive overheat ratio is employed, defined as

$$a_R = \frac{R - R_0}{R_0}, \tag{3.2}$$

where R_0 is the resistance at ambient temperature (cold resistance) and the actual resistance, R, is given by

$$R = R_0[1 + \alpha(T - T_0)], \tag{3.3}$$

α being the temperature coefficient of resistivity. This parameter is important since it determines the temperature of the hot-wire and the sensitivity to exterior temperature changes. The system employed an overheat ratio of 1.32 to take shear stress measurements.

In order to have a dynamic Wheatstone circuit bridge it is necessary to introduce an offset voltage. As indicated in figure 3-5, the voltages V_1 and V_2 are the inputs to the amplifier, which will have a zero output if the input difference is zero. Therefore, it is necessary to establish an operation point using an offset voltage which establishes a mean current through the sensing element. A method to introduce the offset voltage is using a bridge bias, V_{offset}. The characteristic damping, natural frequency and stability of the system are functions of the

voltage offset [2].

The voltage output could be offset by a desired amount using the offset knob indicated in figure 3-8. In order to minimize errors when offsetting the voltage, the gain value was set to 20, and the output knob (see figure 3-8) to channel 0 before offset. Channel 0 provides the (bridge voltage + offset)*gain signal. More specifically, if you wish to operate with an output voltage of V_0= 0 V for certain flow conditions with a gain value of 1, you will use the offset to adjust the output from channel 0 to the value $V_0 = 0$ V. However, if after adjusting the offset you have an error of 1 mV and decide to change the gain to a higher value, the error will be amplified by a factor equal to the gain value. The resulting output signal from the hot-wire can be amplified using the amplification octal switch indicated in figure 3-8. Amplification values up to 200 are possible, the experiments employed an amplification value of 20.

Finally, a cut-off frequency for the signal from the sensing element can be specified by means of the signal filtering switch indicated in figure 3-8. The system has cut-off frequencies between 500 Hz and 20 kHz. In order to reduce the noise introduced by the IOS motor, the 500 Hz filter was used when acquiring measurements.

3.2.4 Sensor calibration

Obtaining measurements in the rotor-oscillator flow requires calibration to transform the voltage signal of the sensing element into shear stress. In order to obtain a quantitative relationship between voltage and shear stress the calibration procedure followed two steps: near-zero shear stress calibration and fixed-position calibration. Both steps are performed in the rotor-oscillator arrangement and employ a FLUENT Navier-Stokes solution of the shear stress for calibration.

The near-zero shear stress calibration determined the voltage value that corresponded to the zero shear stress location. In steady state, fluid flow at the zero shear stress point is transverse to the wall. Although the boundary sidewall is flush with the sensor, its finite size results in heat transfer to the fluid at the zero shear stress location. More explicitly, zero shear stress does not correspond to a zero voltage reading and requires a systematic procedure for calibration. Additionally, the sensing element is perpendicular to the two-dimensional plane where motion occurs, and unable to determine flow directionality [11]. Therefore, the voltage corresponding to the zero shear stress location is a minimum and is mathematically discontinuous. Figure 3-9

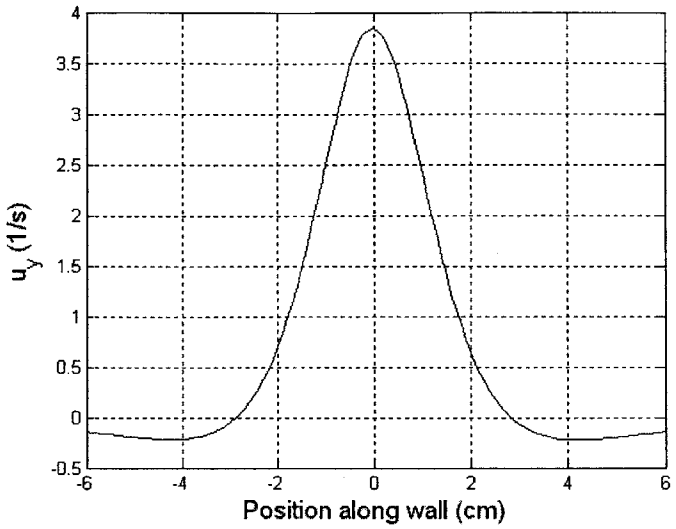

Figure 3-9: Shear stress on the wall calculated utilizing FLUENT. The simulation was performed at an angular rate $\omega = 60$ rad/sec, and cylinder separation from cylinder $c = 2.5$ cm.

shows a FLUENT shear stress profile and figure 3-10 shows how the FLUENT profile would appear when measured with the hot wire.

Because of the physical constrain of the sensor, it is necessary to have a near-zero shear stress calibration. The procedure comprised determining the zero shear stress location guided by numerical simulation and experimental verification, and moving the rotating cylinder to fixed positions where voltage values for low shear stresses are obtained. In figure 3-11 the data obtained in a near-zero shear stress calibration is shown. The figure shows voltage values at four different distances from the rotating cylinder. The smallest voltage value corresponded to the zero shear stress point, located 2.8 cm away from the cylinder. This result was first obtained using a FLUENT simulation, then was verified experimentally. Immediately after the zero shear point measurement, the rotating cylinder was displaced 2 mm towards the sensor, thus the distance separating the two became 2.6 cm. The cylinder remained in its new still position and a new voltage measurement was acquired. This procedure was repeated until the distance separating sensor and cylinder was 2.2 cm or 2.0 cm. Because of momentum diffusion and thermal equilibration, the voltage measurement at each point was taken over a 3 minute

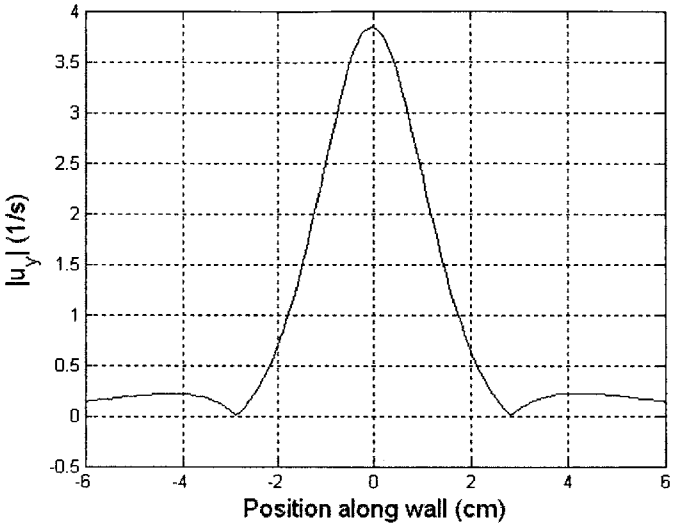

Figure 3-10: Expected output of shear stress sensor at $\omega = 60$ rad/sec and $c = 2.5$ cm.

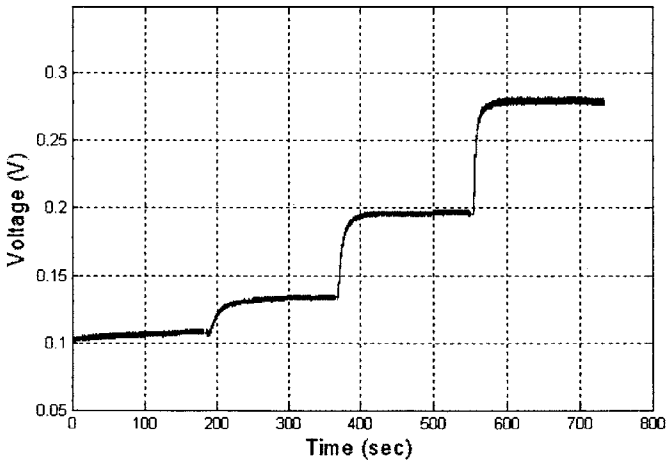

Figure 3-11: Near zero shear stress calibration. The rotor has angular rate $\omega = 60$ rad/sec, cylinder separation from wall $c = 2.5$ cm. Experiment performed using glycerol as working fluid.

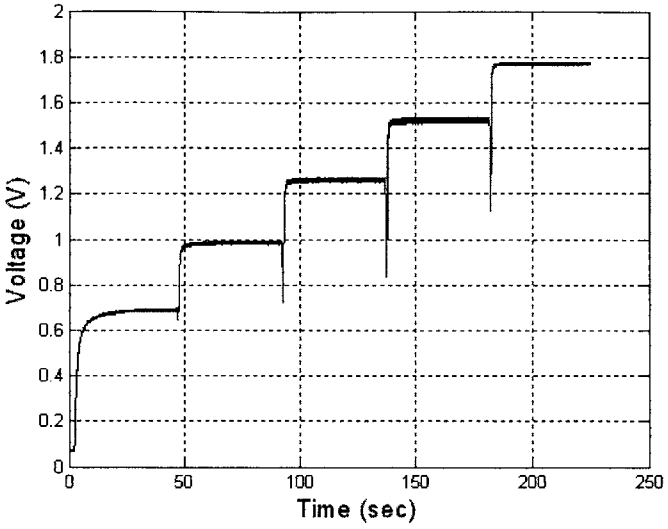

Figure 3-12: Fixed position calibration for sensor. The cylinder is right above the sensor. The sensor undergoes calibration at different angular velocities. The distance of the cylinder from the wall $c = 2.5$ cm.

period to obtain a steady state value. As a result the calibration of one sensor lasted 15 minutes and voltage drift in the sensor became important.

During a 30 minute period, voltage drift in the sensor ranged between 10 and 40 mV. These values corresponded to 5 to 30 % error when measuring shear stress values of the order 10^{-1}Pa at the vicinity of the zero stress location (see figure 3-16). Thus, in order to obtain accurate measurements only one sensor was employed to obtain shear stress profiles so that the time of calibration is minimized as well as the amount of drift in the signal.

While the near-zero calibration was useful to measure low shear stress values located away from the rotor, the fixed-position calibration was faster and more accurate for shear measurements close to the cylinder. In figure 3-12 the voltage measurements for calibration in a fixed position are shown. To continue calibrating the sensor after the near-zero calibration, the second step consisted of bringing the cylinder over the sensor and keep the position fixed throughout the test. The cylinder was then rotated at constant angular speed until the flow over the sensor reached steady state. Once the transients disappeared, the cylinder changed its angular velocity to a higher value almost instantaneously, then this procedure was repeated until the peak

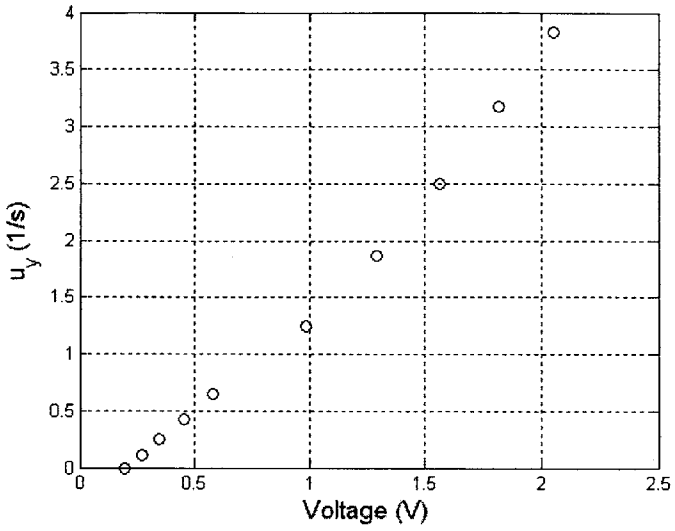

Figure 3-13: Calibration curve utilized to take shear stress measurements.

angular velocity was reached. An example set of results are presented in figure 3-12 in which the cylinder starts the calibration with $\omega = 20$ rad/sec, and finishes the calibration with $\omega = 60$ rad/sec.

Following the data acquisition steps the calibration continues by comparing the voltage values with shear stress values computed numerically utilizing FLUENT. The numerics simulate the experiments performed and assign a shear stress values to every point considered in the calibration. The details of the numerical simulation are explained in section 3.3. A typical calibration utilized in the experiments is shown in figure 3-13. The first five calibration points correspond to the near-zero shear stress calibration while the higher points correspond to the fixed position calibration.

Sensor time response under flow conditions

The characteristic time scales for the transient behavior in a fixed position calibration can be seen in figure 3-14. As a result of a step change in angular velocity, the response of the sensor shows to be almost instantaneous. The characteristic time scale for adjustment agrees with the

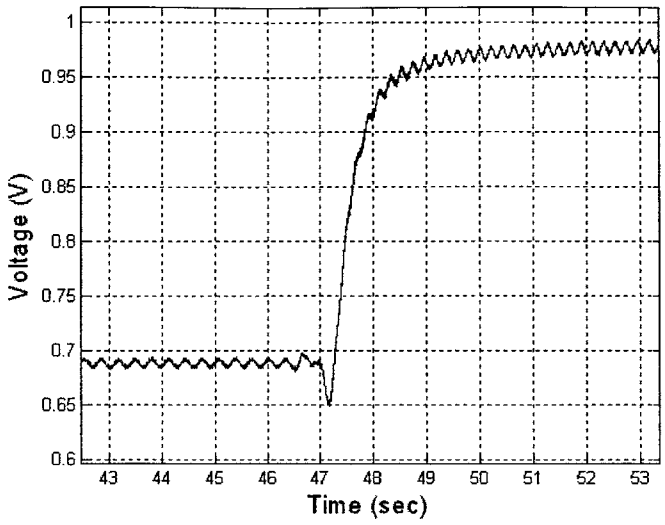

Figure 3-14: Transient response of the shear sensor when applied a step change in angular velocity. The rotation rate is changed from $\omega = 20$ rad/sec to $\omega = 30$ rad/sec.

momentum diffusion time scale defined as

$$\tau_d = \frac{L^2}{\nu} \tag{3.4}$$

where L is a characteristic length, and ν is the kinematic viscosity. The calibration curve shown in figure 3-14 was obtained for a cylinder distance from the wall $c = 2.5$ cm using glycerol as working fluid. The time scale, τ_d, that momentum takes to diffuse from the cylinder to the wall is approximately 0.6 sec. In figure 3-14, the sensor takes 0.9 sec to adjust its response to the step change in angular velocity. In the lower and upper portions of the step, the frequency of the oscillatory signal corresponds to the rotational frequency of the cylinder at which calibration took place, in this case 20 and 30 rad/sec. These results imply that at large velocities the sensor was able to follow the flow field.

Comparing the average value of the voltage with the amplitude of oscillatory noise, it is clear that the error introduced by the cylinder geometry and alignment is small. The typical noise due to geometry and alignment was of the order of 1 %. On the other hand, figure 3-11 demonstrates that the transients for the near-zero calibration are dramatically longer. This

behavior suggests that because of the slow velocities of the fluid away from the cylinder, the heat transfer rate is dramatically decreased, augmenting the transient behavior. In view of this, shear stress measurements in high frequency flows were not performed since the time scale at which the flow field is changing is much faster than the time scale at which the sensor responds.

3.3 Numerical techniques for flow simulation

In order to perform the numerical simulations two resources were utilized: numerical solution by means of the commercial software FLUENT; and the analytical solution obtained by Hackborn, presented in the second chapter of the present work [6]. In the simulation performed using FLUENT, the rotor-oscillator arrangement was modeled as a two dimensional flow with stationary and moving wall boundary conditions. The stationary wall boundary condition models the tank walls, while the moving wall boundary condition represents the rotation of the cylinder. The geometry considered for the model was a plane of 40 cm in length and 10 cm in width thus resembling the tank cross section. In this two-dimensional plane the cylinder reduces to a circle with a radius of 3 mm. To obtain an accurate description of the flow field, the mesh generated in the FLUENT contained 480000 elements. The tank wall, where separation occurs, was partitioned in segments of 1 mm; the remaining walls were partitioned in elements of 5 mm, and the cylinder circumference representing the rotor was divided in segments of 0.5 mm resulting in a fine resolution for the region of interest. The geometry was meshed using a Tri type mesh. The equations solved were the full two-dimensional incompressible Navier-Stokes equations. The residual error for the steady state solution was of the order of 10^{-4}. The FLUENT model has advantage over the solution provided by Hackborn since the size of the cylinder that drives the motion is explicitly modeled [6].

The analytical solutions by Hackborn, discussed in chapter 2, can be evaluated by using numerical integration. In order to reduce computational time a Gaussian Quadrature was utilized. This method showed convergence of the flow field solution. In order to obtain information of other physical quantities such as shear stress and pressure distribution on the tank walls, standard finite difference schemes were employed. The results obtained via Hackborn solution were compared to simulations performed by the commercial software FLUENT. There was a

close agreement in the results for the experiment configurations modeled as steady.

3.3.1 Hackborn solution using Gaussian quadrature for integration

Gaussian Quadrature provides an approximation for an integral by choosing the optimal abscissa to evaluate the function to be integrated. The abscissas are computed from the roots of the Legendre polynomials of order n, $P_n(x)$. These polynomials have the properties of being orthogonal, having all its roots in the interval $[-1, 1]$ and being symmetric with respect to 0.

In general, the integral of the function $f(x)$ over the interval $[a, b]$ can be evaluated from

$$F(x) = \int_{-1}^{1} f(x)dx = \sum_{i=1}^{n} w_i(\hat{x}_i)f(\hat{x}_i) \tag{3.5}$$

The right hand side contains the integrand evaluated at the roots of the Legendre polynomial of order n, and a weighting function for every polynomial root. In order to apply the Gaussian Quadrature it is necessary to change the original integration interval $[a, b]$ to the interval $[-1, 1]$, which is the interval where the Legendre polynomial roots live. Both the weighting function values and roots of the Legendre polynomial of any order n can be found in mathematical tables.

The integration of equation (2.20) showed convergence for Legendre polynomials of increasing order. The region of integration was near by the flow separation point of the sidewall at a distance $c = 0.5$ from the cylindrical rotor. The exact solution was assumed to be that computed from the Legendre polynomial of degree $n = 20$. The solution of the entire flow field for the rotor configuration was obtained with a Legendre polynomial of order $n = 14$.

3.3.2 Steady solution for rotor-oscillator experiment

The solution provided by Hackborn yields the entire velocity field of the rotor experiment. The velocity field allows visualization of separation regions near the wall, as can be seen in figure 3-15. The velocity field shows that the momentum provided by the rotor decreases very rapidly when moving away from the rotor. The characteristic velocities of the flow at the sidewalls are slow, of the order of 0.5 mm/sec, and therefore particle departure from the sidewall occurs at large time scales.

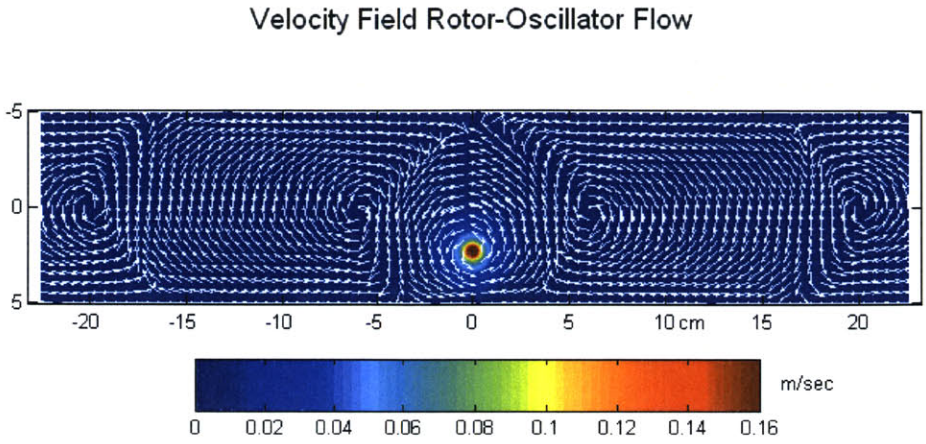

Figure 3-15: Steady solution for rotor-oscillator flow utilizing Hackborn's solution.

It is also of interest to quantify other physical notions such as shear stress and pressure. In Haller's kinematic theory [10], flow separation can be predicted from the shear stress and pressure distributions over the surface. In the steady rotor-oscillator experiment the shear stress and pressure were computed at the sidewall located at $x = 1$. Hackborn explored the steady separation in the rotor experiment utilizing Prandtl criteria [8] given by equations (1.4) and (1.7). The results obtained by Hackborn [8] are shown in Table 3.1 along with their comparison to the results obtained in the present work using a Gaussian quadrature. The results are shown using dimensionless quantities defined in chapter 2. A difference on the order of 2% was found. There are two separations points; the first separation point is of greater interest since the characteristic flow velocities are of one order of magnitude bigger than those in the far separation point; therefore, the measurement of shear stress and pressure distribution is more

Rotor position c	0.25	0.441	0.5	0.75
Hackborn separation points	0.906	0.681	0.599	0.267
	3.648	3.297	3.137	2.374
Calculated separation points	0.919	0.694	0.611	0.276
	3.66	3.31	3.151	2.388

Table 3.1: Dimensionless separation point for rotor-oscilator flow

accessible to current sensor technology.

The shear stress and pressure distribution were computed utilizing standard finite difference schemes. The numerical schemes are accurate up to second order. The results were compared to simulations run in the commercial Navier-Stokes solver software FLUENT and are shown in figures 3-16 and 3-17. The solutions for the shear stress provided by both methods, Hackborn and FLUENT, differ on the order of 10^{-2} Pa. In addition, the zero shear stress point, or point of steady flow separation, is different on the order of millimeters. The result obtained for the pressure distribution differs on the order of 10^{-1} Pa.

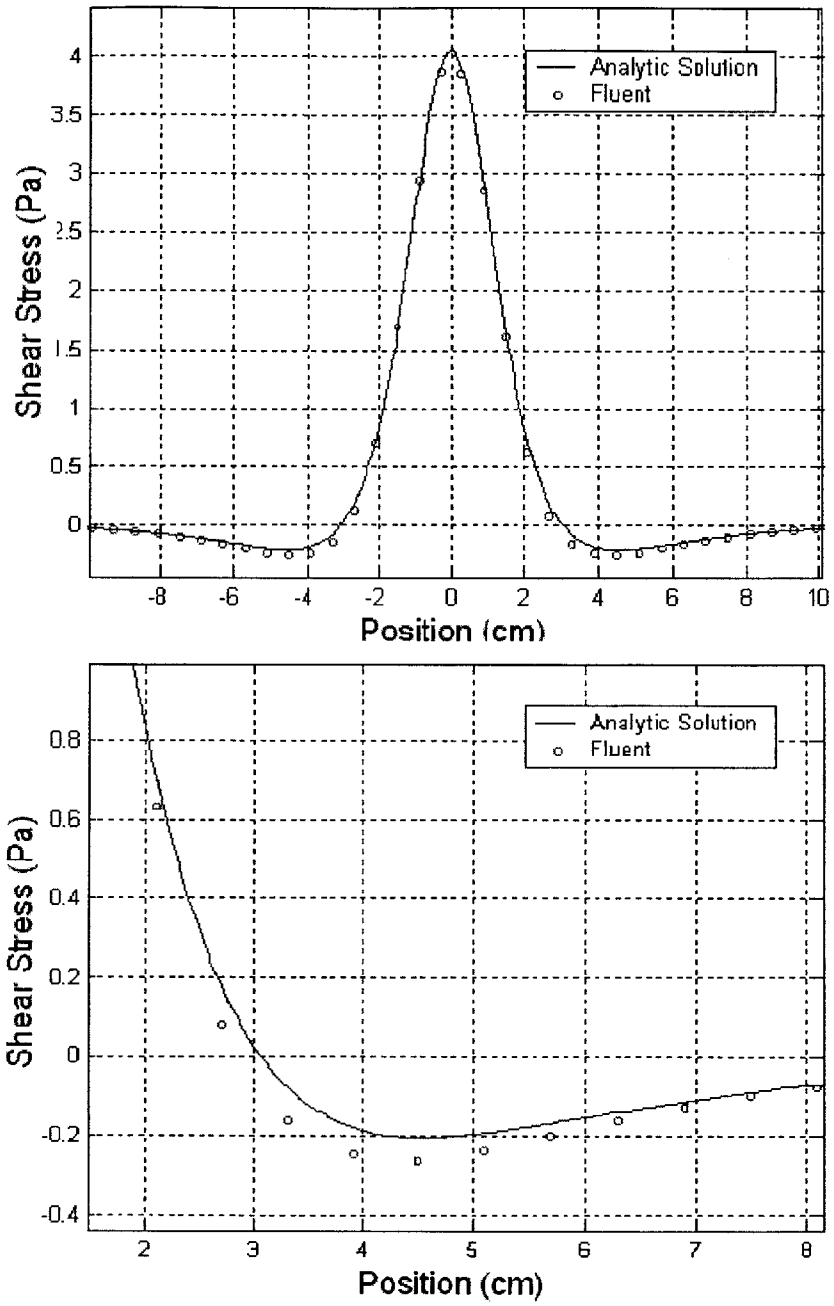

Figure 3-16: Shear stress at wall predicted by FLUENT and Hackborn analytic solution.

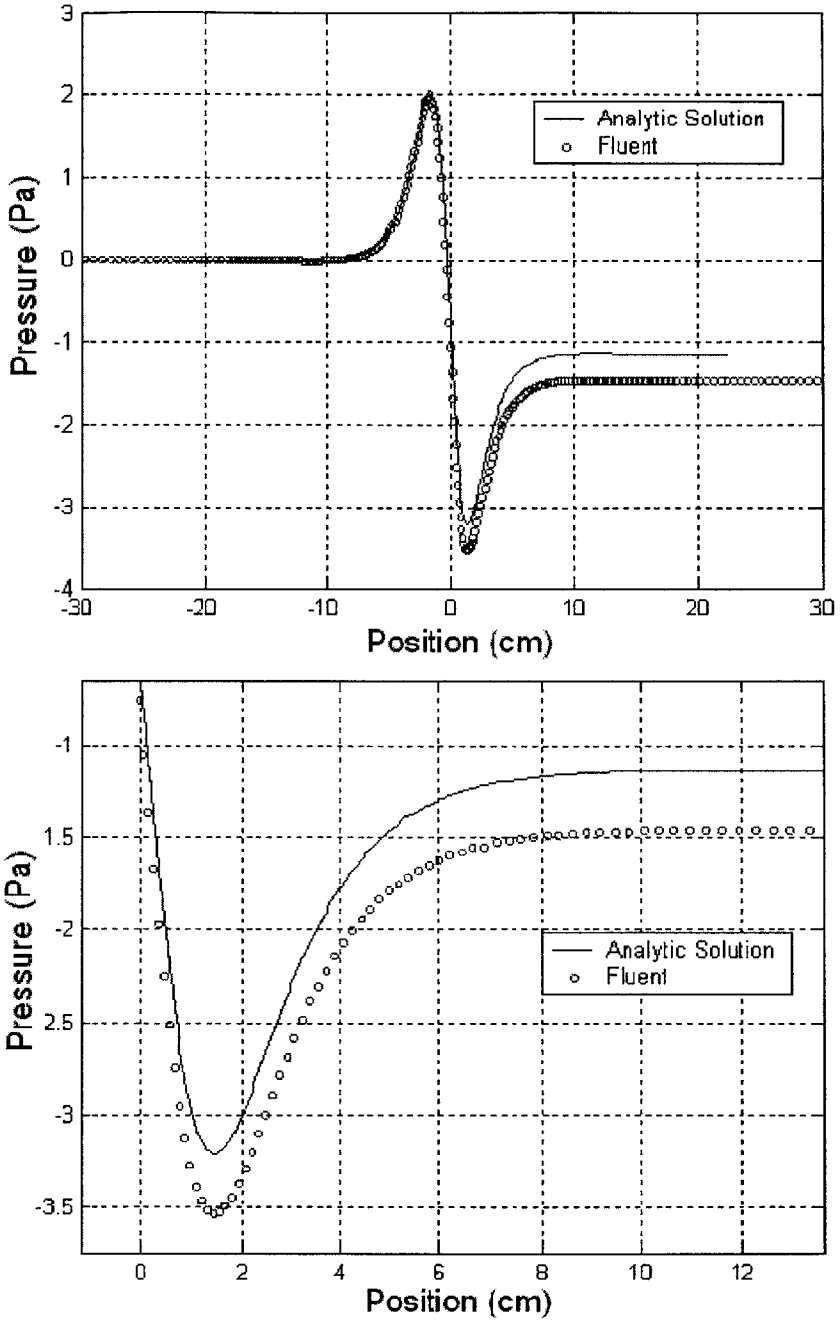

Figure 3-17: Pressure at wall predicted by FLUENT and Hackborn analytic solution.

Chapter 4

Fixed separation in steady flows

Fixed separation occurs when fluid particles are ejected to the main stream from a fixed position on a boundary wall. In steady flows, fixed separation follows a time independent separation profile rooted at a single point on the wall, the fixed separation point. In this chapter, the existence of this separation point in the rotor-oscillator arrangement is investigated experimentally and numerically.

The experiments sought to verify that the rotor-oscillator flow fulfills the functional requirements to validate the separation criteria. The experimental work employed two methods to characterize flow separation: flow visualization, and measurements of wall shear stress. The former method is direct and explicitly shows where flow separates from the boundary wall. The latter method is indirect and infers flow separation through the theory developed by Haller [10]. Supporting numerical simulations used FLUENT commercial software to investigate the steady flow field properties. Flow separation in these simulations was determined by either numerical particle tracking or via Haller's separation criteria [10].

4.1 2D Nature of the rotor-oscillator flow

The theory considered in chapter 1 applies to general unsteady two-dimensional flows. The rotor-oscillator flow is an arrangement where three dimensional effects are minimized by choosing a relatively large width to depth ratio of the tank, and focusing on fluid flow in a plane between the base and free surface of the tank. The length of the tank was four times the width

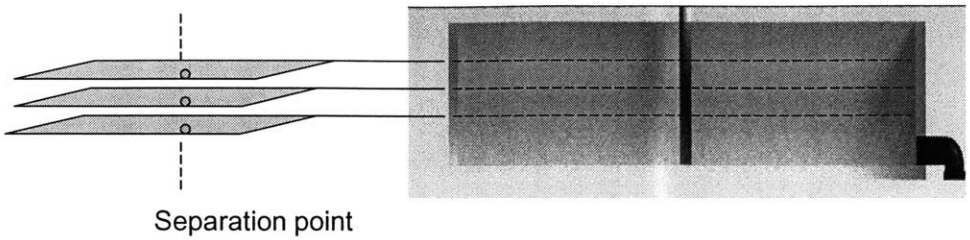

Figure 4-1: Flow separation points occurring at same location in flow planes at different depths.

and flow visualization in these experiments was performed at a depth of 4.5 cm, as measured from the free surface (the tank depth is 12 cm). Intuitively, it would seem that the best region to perform flow visualization is the center of the tank, which would be the case if the boundary conditions were the same at the top and bottom of the tank. This was not the case in the rotor-oscillator experiment, as the bottom enforced a zero velocity condition whilst the top was a free surface. As such, we found motion to be most two-dimensional in a plane 4.5 cm below the free surface.

To label the flow as two-dimensional the velocity field occurring at different depths must be identical and no mass flux should occur between horizontal planes. Therefore, in a two-dimensional flow it is necessary that the separation point at different depths of the tank occurs at the same position, thus implying that the planar velocity fields at different depths are nearly identical. Figure 4-1 portrays different flow planes in which fluid separates at the same location.

With the purpose of verifying the flow two-dimensional nature, the point of flow separation at different depths along the length of the cylinder was measured. Material lines of dye were placed along the wall at different depths in the tank, as measured from the free surface of the fluid. The cylinder had a constant angular velocity, $\omega = 60$ rad/sec, giving a Re $= 0.46$ as defined in equation (2.5). The parameters utilized in these experiments are summarized in table 4.1. The experiments were performed at 18 ± 0.1 C, corresponding to a 3 % viscosity

$\mathbf{Re} = \frac{r^2\omega}{\nu}$		$\mathbf{Sr} = \frac{h^2\alpha}{2\pi r^2\omega}$	
r	3 mm	α	0
ω	60 rad/sec	h	5 cm
ν	1.2×10^{-3} m^2/s	A (no oscillation)	0 cm

Table 4.1: Experimental parameters to verify the 2D nature of the rotor oscillator flow

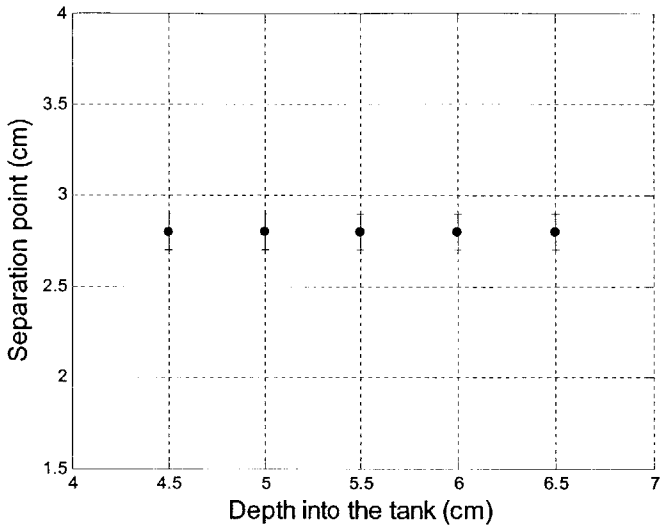

Figure 4-2: Separation point at different depths of the fluid tank. Re = 0.46.

fluctuation. This thermal fluctuation is expected to be irrelevant to the dynamics of the flow since the Re number for the flow is well in the Stokes regime.

The region of the tank where material lines of dye remained in a two-dimensional plane lay between 6.5 cm and 4.5 cm depth. Outside this range, flow visualization revealed three-dimensional trajectories of the material line of dye. Small three-dimensional effects are expected because of the non-slip boundary condition at the bottom of the tank and the free surface on the top. However, by considering the regions near the center of the tank, the visualizations indicated that there was indeed a robust two-dimensional flow in the rotor-oscillator configuration suitable for studying unsteady flow separation.

It was observed that separation occurred at a fixed point in the wall at the same location for different flow planes between 4.5 cm and 6.5 cm. In figure 4-2 the visualization results are presented. The separation point was measured to occur at 2.8 $\pm$0.1 cm from the position of the cylinder. There is an uncertainty in the measurements caused by the finite width of the separation profile. At the location where separation takes place, flow was drawn into the separation profile whose base was anchored at the wall. The width of the dye attracted to the separation profile generated an uncertainty of $\pm$1 mm, as shown in figure 4-3.

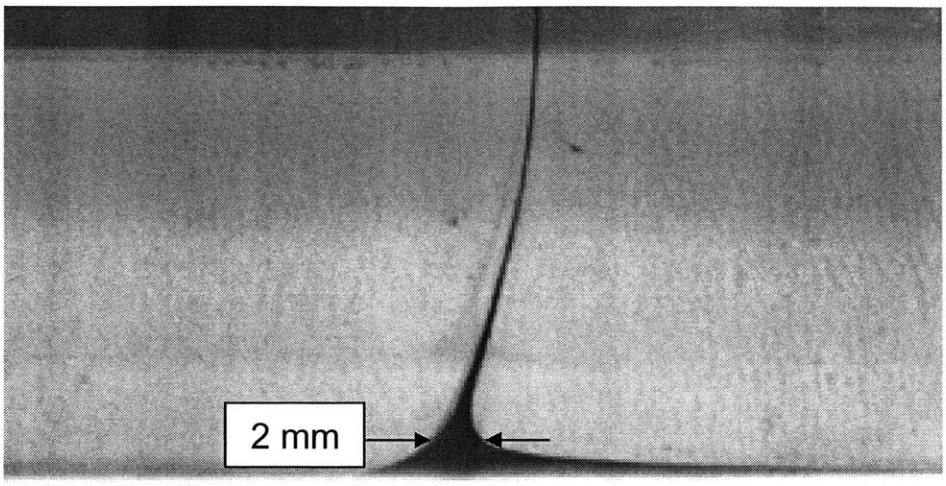

Figure 4-3: Separation profile for steady flow at Re = 0.46. The profile has a finite width resulting in uncertainty when measuring the separation location.

4.2 Separation in steady flow

Flow separation in steady flows has been demonstrated to occur at the position of vanishing skin friction along the boundary wall. The theory Prandtl developed in 1904 provided a set of criteria given by equations (1.4) and 1.7) that describe separation in steady flows [17]. In the rotor-oscillator flow with no translational motion of the cylinder, the flow is steady and separation occurs at the point of zero skin friction. Hackborn [8], studied the location of flow separation for the steady rotor-oscillator experiment and compared these results to the analytical solution for the flow field developed in his previous work [6]. Previous work by Hackborn indicates that for Re numbers of order of unity the separation point does not depend on the angular velocity of the cylinder and shows strong correlation to the cylinder distance from the wall [8]. In the present experiments the location of the flow separation is studied and compared with the Hackborn analytical solution and numerical simulations performed using the commercial software FLUENT. Additionally, the location of the separation point is studied as a function of the rotational speed of the cylinder and its distance from the wall. The flow considered in the experiments of this section had Re = 0.46.

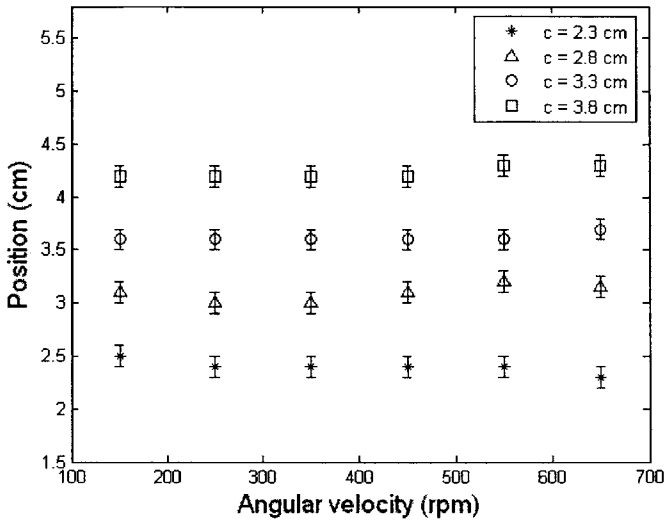

Figure 4-4: Separation point location in steady state flow determined utilizing dye visualization. 1 rpm is equivalent to $\pi/30$ rad/sec.

4.2.1 Experimental results utilizing flow visualization

Varying the rotation rate of the cylinder and its distance from the wall, the separation point location was measured. The point of separation was visualized by drawing material lines of dye 4 cm to 5 cm in length along the wall, and observing the separation locations. The wall separation from the cylinder was limited to 3.8 cm; for greater separations of the wall the visualizations revealed that the velocity field was not well confined to a two-dimensional plane. Experimental runs were each performed in nearly constant temperature conditions. The temperature range for the experiments was between 17 C and 19 C and the temperature variation during an individual experimental run was ± 0.1 C.

In figure 4-4 the experimental data is presented. The results show that there is not significant variation of the separation point as the angular velocity is increased. For example, for $c = 3.5$ cm the location of separation remained at 3.6 cm over a range of angular velocity between 150 rpm and 650 rpm or 15.7 rad/sec to 68.1 rad/sec. Recalling the definition of the Re for this flow, $\mathrm{Re} = \frac{r^2\omega}{\nu}$, it is clear that the Re number of this flow does not affect the location of the separation point. On the other hand, the location of the separation point possesses a

quasi-linear dependence on the distance of the cylinder from the wall.

4.2.2 Numerical simulations compared with experimental flow visualization

In order to visualize flow separation from a surface, particle tracking was used in the numerical simulations. In the rotor-oscillator experiment separation occurs at the sidewall closer to the rotor. For the steady separation profile, the rotor is not oscillating and therefore there is no change of the flow field properties with time. Placing particle seeds in the vicinity of the walls allows following the trajectories that such particles take as time progresses. To simulate particle tracking in the flow the Hackborn solution was employed, whilst shear stress on the wall was obtained using FLUENT.

To visualize how the fluid particles behave near the separation point, a material line of particles was placed near the boundary wall. As can be seen in figure 4-5, the separation profile formed and remained unchanged. The particle seeds are attracted towards the separation point and then ejected and stretched, forming the separation profile.

The comparison of the numerical and experimental results is shown in figure 4-6, in which the results of numerical particle tracking are compared directly with the experimental results in figure 4-4. The ratio of the location of separation predicted by the numerics and the value experimentally measured is on the y axis while the Re number is on the x axis. In the Re number the fluctuation of the viscosity with temperature has been accounted for. The simulations performed by FLUENT differ in the location of separation by about 1 mm to 2 mm, which represents an error of 5 %. The analytical solution was corrected to closely match the experimental results for different angular velocities and cylinder distance from the wall.

Finally in figure 4-7, we present a direct comparison between the experimental and numerical separation profiles utilizing Hackborn's solution for $\omega = 60$ rad/sec and $c = 2.8$ cm. The location of separation agreed within 1 mm, however, the slope of the separation profile was different. This can be attributed to inertial effects that were not accounted for in the particle tracking performed utilizing the Hackborn solution, or to three-dimensional effects.

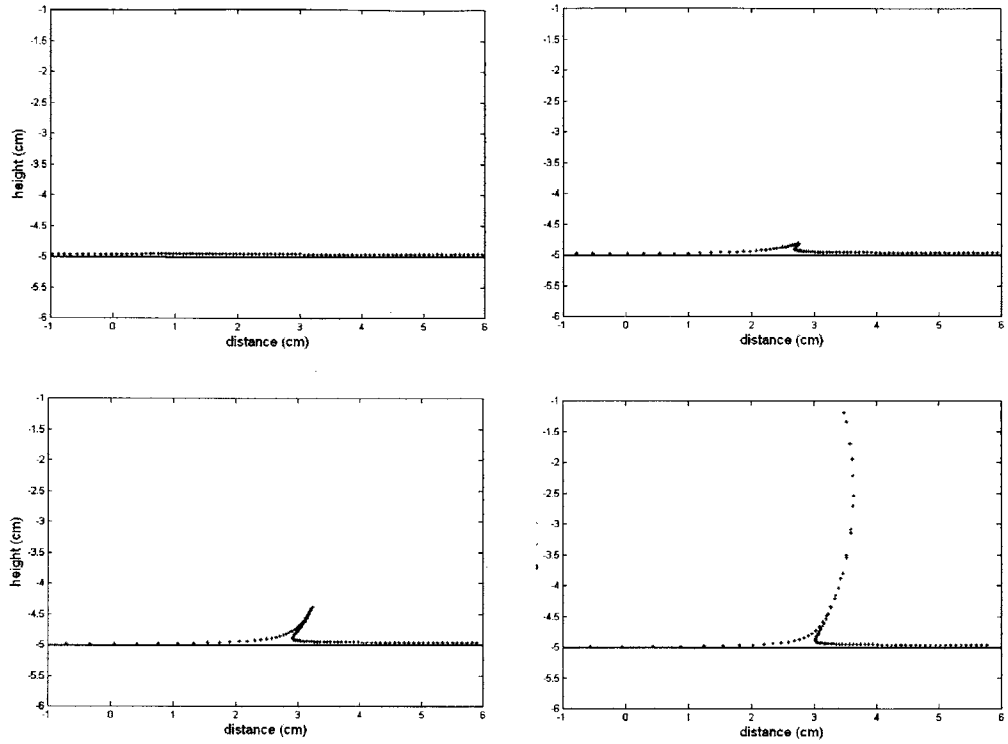

Figure 4-5: Numerical visualization of separation in steady flow by using a material line. Once the separation profile was formed it remained unchanged for all times. The simulation was perfomed using an angular rate $\omega = 60$ rad/sec and distance of the cylinder from the wall $c = 2.5$ cm. The particle tracking was performed using Hackborn's solution.

4.2.3 Comparison of numerical results with separation inferred from shear stress measurements

In order to demonstrate the practicality of the separation criteria by Haller [10], the shear stress sensor system described in chapter 3.4 was utilized to acquire measurements on the wall. The measurements are used to determine flow separation using equation 1.1, and compared with the numerical results. All measurements were acquired under the same flow conditions; the parameters chosen were angular rate $\omega = 30$-60 rad/sec and distance of the cylinder from the wall $c = 2.5$ cm. Because of the constant viscosity of glycerol under low shear rates, all the

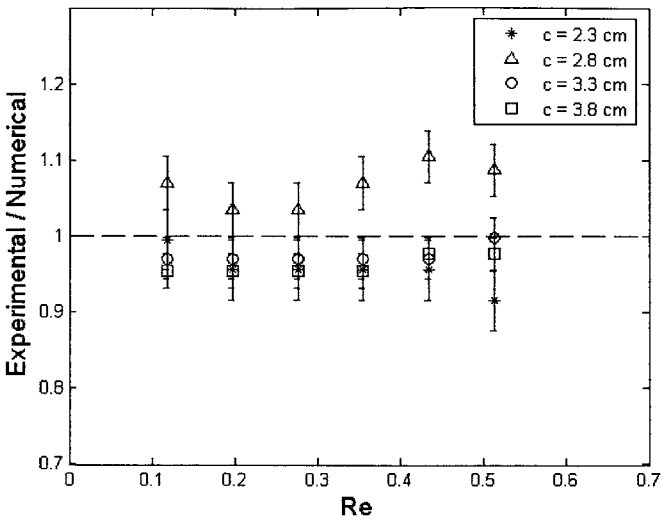

Figure 4-6: Comparison between numerical simulation using FLUENT and experimental measurements in the steady rotor-oscillator flow.

tests employed glycerol as working fluid.

Utilizing both dye visualization and shear stress the separation point at steady state was determined and the results are shown in figure 4-8. The visualization and shear stress measurements agreed to within experimental accuracy. The flows were simulated numerically, and a comparison between the experimental measurements and simulation is shown in figure 4-9. The agreement between experiment and simulation has an error smaller than 2 %.

Finally, we measured the experimental shear stress profile for the steady flow. In order to construct the profile, measurements were taken using a single sensor. For all tests, the sensor was fixed at a determined wall position and the cylinder translated to different locations, changing its position relative to the sensor. Since the lateral walls of the tank are far away from the region of interest and the Re is small, their effect in the flow field was negligible, making this approach possible. To minimize the effect of sensor drift, at every point where a measurement was taken a new sensor calibration was performed. The comparison between numerical simulation and experimental data is shown in figure 4-10. Overall, there is good agreement between numerical and experimental data.

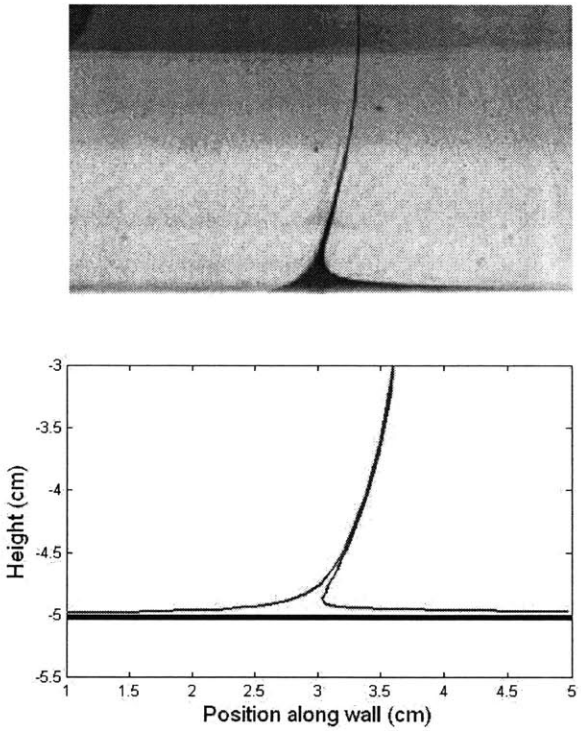

Figure 4-7: Separation profile in the rotor-oscillator flow. The angular velocity $\omega = 60$ rad/sec, distance of cylinder from the wall $c = 2.5$ cm. Particle tracking was performed using Hackborn's solution.

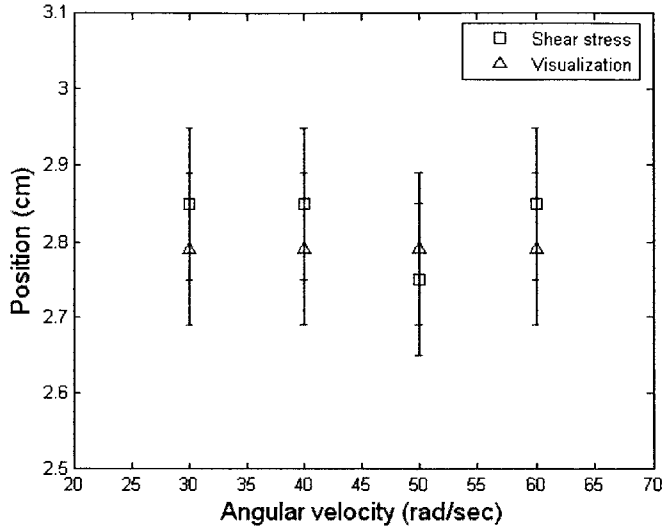

Figure 4-8: Steady separation measured utilizing dye visualization and shear sensors. The distance of the cylinder from the wall $c = 2.5$ cm.

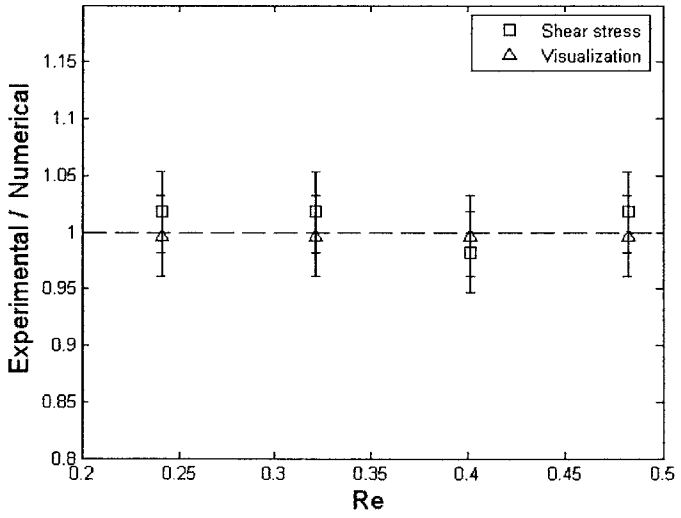

Figure 4-9: Steady separation measured utilizing dye visualization and shear sensors compared to FLUENT simulations. The distance of the cylinder from the wall $c = 2.5$ cm.

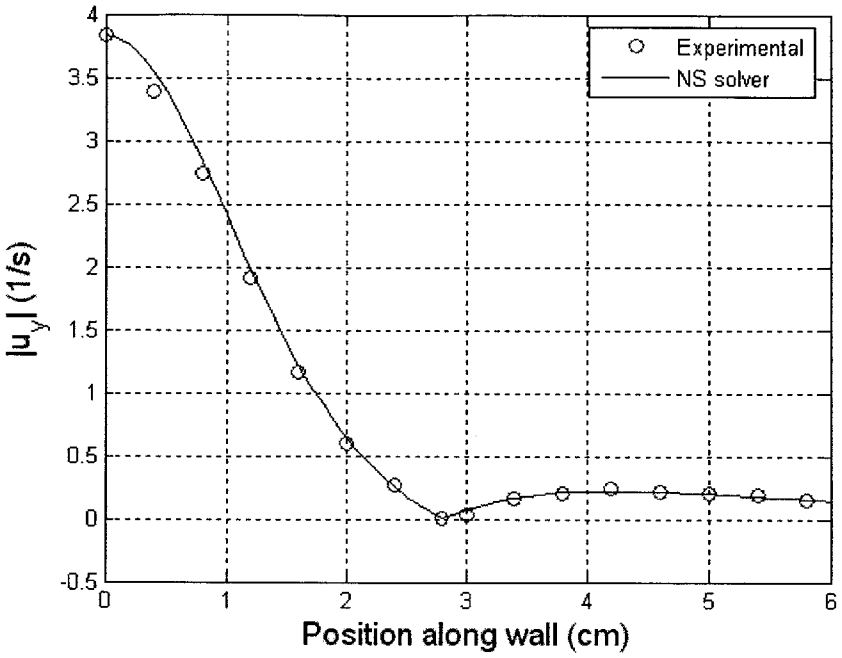

Figure 4-10: Comparison between experimental and numerical shear stress obtained using FLUENT. The parameters are $\omega = 60$ rad/sec and $c = 2.5$ cm.

The experimental shear measurements, flow visualizations, and numerical simulations presented in this chapter show that the rotor-oscillator flow was indeed a two-dimensional flow, where separation occurs on observable time and length scales. The presented data are also consistent with the notion that in a steady incompressible flow separation occurs at the point where the shear stress vanishes, following Prandtl's separation criteria.

Chapter 5

Fixed separation in unsteady flows

Fixed separation in unsteady flows can be observed under periodic time dependence of the flow field. In an incompressible periodic flow, previous work by Shariff et al. [22] demonstrated that flow separation occurs at a fixed separation point, and that the instantaneous zero skin friction point does not indicate the location where fluid flow departs from the boundary. The theoretical developments were corroborated by the experimental work of Hackborn [8], who explored the effect of periodic time dependence in the rotor-oscillator flow.

A significant advance of the theory of fixed separation in periodic flows has been developed by Haller [10]. The formulation covers compressible flows, and furthermore predicts the existence of fixed separation points in aperiodic as well as periodic flows, provided there is a long term zero mean skin friction point.

In the work presented here the flow field was incompressible, and the unsteady flow conditions were produced by translation of the cylinder in the rotor-oscillator flow. Specifically, time-periodic flow in the experiments was obtained by sinusoidal translation of the cylinder whilst aperiodic flow conditions were produced by a random-type translation of the cylinder.

5.1 Theoretical treatment of fixed separation in unsteady flow

Fixed separation can occur in periodic or aperiodic flows. The location of a fixed separation point in an unsteady flow field can be determined using the criteria developed by Haller [10],

which are described in section 1.4 and recapitulated here. The location of separation γ satisfies

$$\boxed{\lim_{t\to-\infty}\int_t^{t_0}\frac{\tau_w(\gamma,0,\tau)}{\rho^2(\gamma,0.\tau)}d\tau=0,} \tag{5.1}$$

$$\boxed{\lim_{t\to-\infty}\int_{t_0}^{t}\left[\frac{1}{\rho(\tau)}(u_{xy}(\gamma,0,\tau)-v_{yy}(\gamma,0,\tau))-2v_{xy}(\gamma,0,\tau)\int_{t_0}^{\tau}\frac{u_y(\gamma,0,s)}{\rho(\gamma,0,\tau)}ds\right]d\tau=\infty,} \tag{5.2}$$

and the slope of separation f_0 is determined by

$$f_0(t_0)=\lim_{t\to-\infty}\frac{\int_{t_0}^{t}\left[u_{yy}(\gamma,0,\tau)+3u_{xy}(\gamma,0,\tau)\int_{t_0}^{\tau}u_y(\gamma,0,s)ds\right]d\tau}{3\int_{t_0}^{t}u_{xy}(\gamma,0,\tau)d\tau}. \tag{5.3}$$

In periodic flows the dynamics of the flow field are fully described in one period of oscillation, thus equation (5.1) reduces to

$$\int_0^T\frac{\tau_w(\gamma,0,\tau)}{\rho^2(\gamma,0.\tau)}d\tau=0, \tag{5.4}$$

where T is the period. Similarly, the slope of separation profile is given by the equation

$$f_0(t_0)=\frac{\int_0^{T}\left[u_{yy}(\gamma,0,\tau)-3u_{xy}(\gamma,0,\tau)\int_{\tau}^{T}u_y(\gamma,0,s)ds\right]d\tau}{3\int_0^{T}u_{xy}(\gamma,0,\tau)d\tau}. \tag{5.5}$$

5.2 Fixed separation in periodic flow

5.2.1 Periodic flow solution for rotor-oscillator flow

Hackborn considered the problem of a rotating cylinder submerged in a rectangular tank with an oscillatory sidewall [5]. The flow behavior was described using the superposition of a steady line rotlet between two parallel plates and a time-periodic Couette shear flow. The superposition principle is possible because in the limit of Re $\ll 1$ and Sr number of $O(1)$ the Stokes approximation holds and the properties of linear systems apply.

The present work considers the analogous situation of a rotating cylinder with oscillatory translational motion in the direction parallel to the sidewalls of a tank. The flow solution is obtained by assuming the flow to behave quasi-steadily. Thus, for small oscillatory frequencies and amplitudes, the solution of the flow at any time can be represented by a steady line rotlet whose origin translates according to the imposed oscillation.

In the experimental arrangement the cylinder is periodically displaced so that the observer in the laboratory frame sees the back and forth periodic motion of the cylinder. The walls of the tank and the observer are stationary in the lab frame. In the frame of the oscillating cylinder it is the walls that move periodically. Thus, in a frame attached to the oscillatory motion of the rotor a flow solution can be obtained from the principle of superposition of solutions. Similar to the approach of Hackborn [6], the problem can be modeled as a line rotlet and an oscillatory Couette shear flow. Using the coordinates shown in figure 2-6, the oscillatory solution for the flow v_1 resulting from motion of the wall located at $x = h$ is given by

$$v_1 = \frac{V}{2}(1 + \frac{x}{h})\sin(\alpha t), \tag{5.6}$$

where V is defined as

$$V = A\alpha. \tag{5.7}$$

A being the peak-to-peak amplitude of oscillation, and α is the oscillatory frequency. Similarly, the oscillatory flow v_2 for the wall located at $x = -h$ is given by

$$v_2 = \frac{V}{2}(1 - \frac{x}{h})\sin(\alpha t). \tag{5.8}$$

Superimposing equations (5.6), (5.8), and a line rotlet yields the solution for the oscillating rotor problem in the frame relative to the rotor. The solution can be written as

$$\frac{dx}{dt} = -\frac{d\Psi}{dy}, \tag{5.9}$$

$$\frac{dy}{dt} = \frac{d\Psi}{dx} + V\sin(\alpha t), \tag{5.10}$$

where Ψ is the line rotlet stream function given by equation (2.20). Equations (5.9) and (5.10) show that in the quasi-steady limit the time dependence can be almost removed by a change of reference frames. The solution in the laboratory frame can be obtained by subtracting the periodic velocity term in equation (5.10) and by imposing the appropriate time dependent translation on the line rotlet origin. The solution is given by equation (2.20), along with the

translation of instantaneous origin coordinates for the rotlet equation

$$y = y_0 - \int_0^t V \sin(\alpha\tau) d\tau = y_0 - V[1 - \cos(\alpha t)]. \tag{5.11}$$

Equation (5.11) translates every point of the steady rotlet solution with the same oscillatory translational motion of the rotating cylinder. This equation states that for sufficiently small amplitude and frequency of oscillation the inertial effects in the fluid are nil. Essentially, the cylinder is moving slowly through a viscous fluid and the flow field at any time t is a replica of the flow field of a previous time; the only property changing in the flow field is the position of the cylinder. The unsteady solution considered neglects the flow field resulting from the translation of the cylinder alone which was found to have no effect on the shear stress field at the boundary.

Associated with the linearity of the problem is that the pressure and shear stress will move quasi-steadily with the periodic forcing introduced by the translating cylinder. This result and the separation criteria developed by Haller, in turn allows determining the location of separation by oscillating the wall shear stress profile with exactly the same time dependence of the cylinder motion [10]. Information only at the boundary wall is required to determine the location of flow separation.

5.2.2 Experimental results

The parameters varied in the periodic flow experiments were the amplitude and frequency of oscillatory translation. The angular velocity, ω, and distance of the cylinder from the wall, c, were kept constant with values of 60 rad/sec and 2.5 cm respectively. The results obtained in the steady regime described in section 4.2, indicate that for small Re numbers ω does not affect the separation point, and therefore we also expected that ω would not play a role in the location of separation for the quasi-steady flow at low Re.

The translational motion utilized was of the type

$$y = \frac{A}{2}[1 - \cos(\alpha t)], \tag{5.12}$$

where A is the peak-to-peak amplitude for oscillation, α the oscillatory frequency, and y is

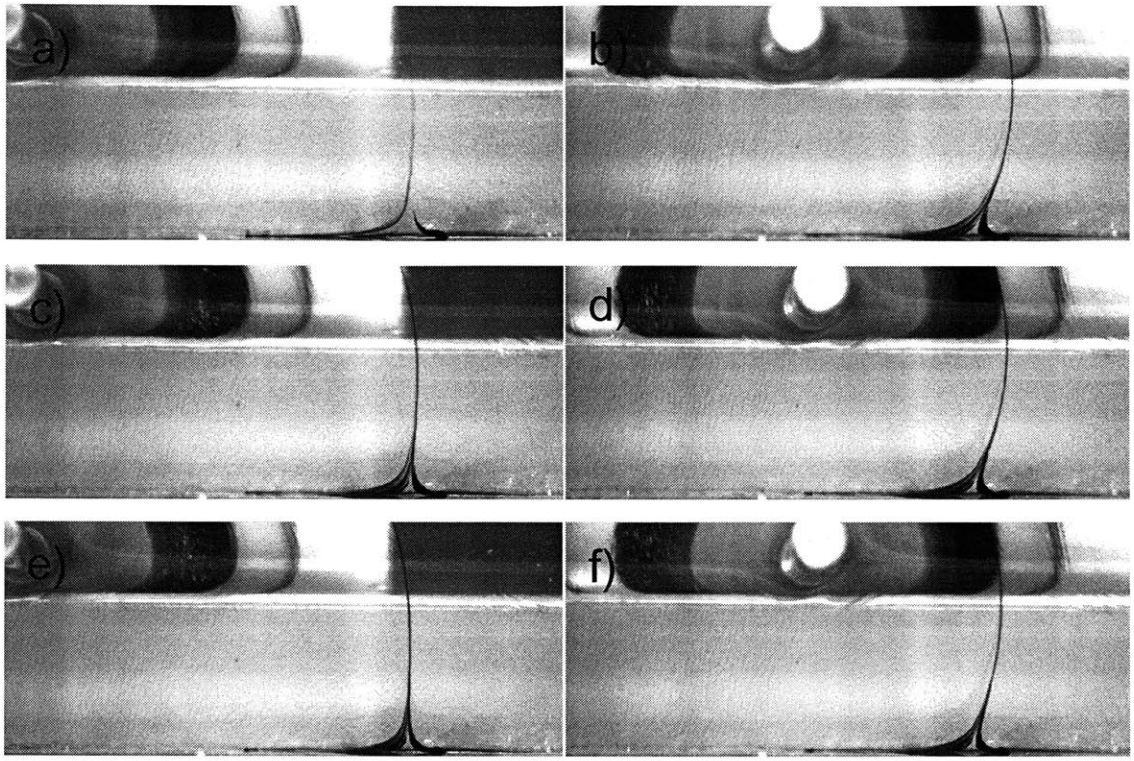

Figure 5-1: Time sequence of fixed separation in periodic flow. The peak-to-peak amplitude of oscillation $A = 3$ cm, the oscillatory frequency $\alpha = 2$ rad/sec. Images are taken at the beginning and at the end of oscillatory motion of the cylinder. Time progresses from left to right and from top to bottom.

aligned with the long axis of the tank. The resulting Re is 0.46 and the Sr number varied between 0.2 and 2. The separation point was visualized by means of streak lines of dye introduced at the boundary wall. There was an uncertainty of ± 1 mm when measuring the location of the separation point due to the finite width of the material line of dye, as shown in figure 4-3. The temperature fluctuations of the experiments resulted in a 5 % change in the Re number through the variation of viscosity

A time sequence of the flow visualizations is presented in figure 5-1. The peak-to-peak amplitude of oscillation $A = 3$ cm and the oscillatory frequency $\alpha = 2$ rad/sec. Flow separation occurred at a fixed location on the wall. The location of separation was 5.0 cm from the origin with an uncertainty of ± 1 mm. In frame 5-1(a) one can observe the cylinder at the origin

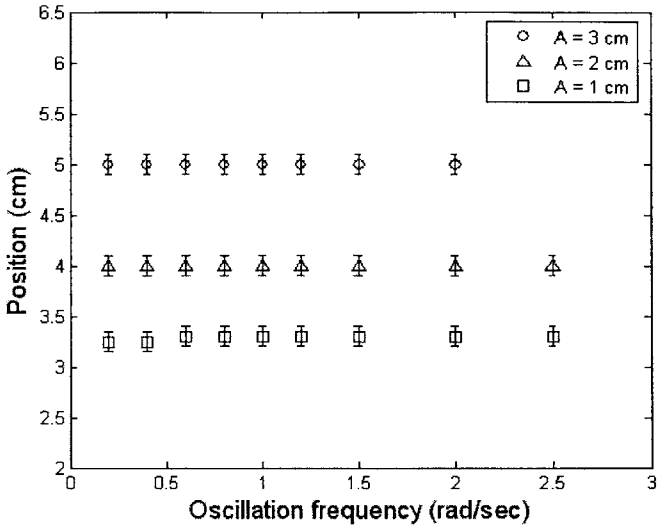

Figure 5-2: Experimental data obtained for fixed separation in a periodic flow using dye visualization.

of the oscillation. Dye starts to be drawn into the separation location, following the unstable manifold or separation profile. Many periods later, frames 5-1(b) to 5-1(f) show the back and forth motion of the cylinder. Flow separation takes place at a fixed position while the separation profile is time dependent. The angle of the separation profile is steeper when the cylinder is at the origin than when the cylinder has reached the end of its forward oscillation.

Measurements of the fixed separation point location for a range of parameters based on dye visualization are presented in figure 5-2. The peak-to-peak amplitude of oscillation A was varied from 1 cm to 3 cm, and α between 0.2 rad/sec to 2.5 rad/sec. Because of limitations in the maximum attainable speed of the mechanical stage to translate the cylinder, a measurement of the separation point in an oscillatory motion with $A = 3$ cm and $\alpha = 2.5$ rad/sec could not be acquired. The location of fixed separation moved away from the cylinder origin as A was increased, and for a set value of A the separation point was insensitive to the frequency of oscillation. This result suggests that the shear stress field in the experimental flow was the same for different oscillatory frequencies and moved quasi-steadily, hence inertial effects did not play a role.

5.2.3 Comparison of flow visualization experiments with numerical simulations

Material lines and streak lines separating from the boundary wall were visualized in a numerical simulation utilizing the periodic solution for the rotor-oscillator flow given by equations (5.9) through (5.11). Additionally, after implementing the criteria developed by Haller the point of flow separation and the slope of the separation profile were determined from the shear stress and pressure distribution on the wall obtained from the Hackborn's solution.

The material line and streak line tracking was performed using information of the entire flow field, while implementing the separation criteria requires information along the boundary wall only. Indeed, according to equation (1.1) locating the separation point in the rotor-oscillator periodic flow requires only determination of the shear stress distribution over the wall. More specifically, at the limit of low Re and Sr the rotor-oscillator flow field at any time is a replica of its steady state flow field, but displaced along with the oscillatory cylinder. Thus, the flow field of the experiment moves quasi-steadily and follows the time dependent forcing of the cylinder. Therefore, determining the shear stress profile in steady state provides enough information to obtain the time dependent shear and determine the separation point via Haller's criteria.

Figure 5-3 shows a time sequence of a material line and streak lines separating from the wall, along with the location of the separation point and separation profile determined via Haller criteria. The simulations in figure 5-3 were performed utilizing Hackborn's solution. To perform these simulations a peak-to-peak amplitude of oscillation $A = 2$ cm, oscillation frequency $\alpha = 5$ rad/sec, and distance of the cylinder from the wall $c = 2.5$ cm were chosen. The streak lines are shown in green, the material line in red, the instantaneous zero skin friction streamline in black, and the predictions using Haller's criteria in blue. The simulations indicate that both material line and streak lines reveal the same location for the fixed separation point under unsteady conditions. Haller's criteria captures the location of separation very accurately. Furthermore, the separation profile agrees at first order with the separation profile observed in simulation. The profile computed via Haller's criteria is a time-dependent linear approximation of the unstable manifold depicted by the material lines and streak lines. The frequency of oscillation for the angle of separation corresponds to the frequency of the oscillatory translational motion of the cylinder.

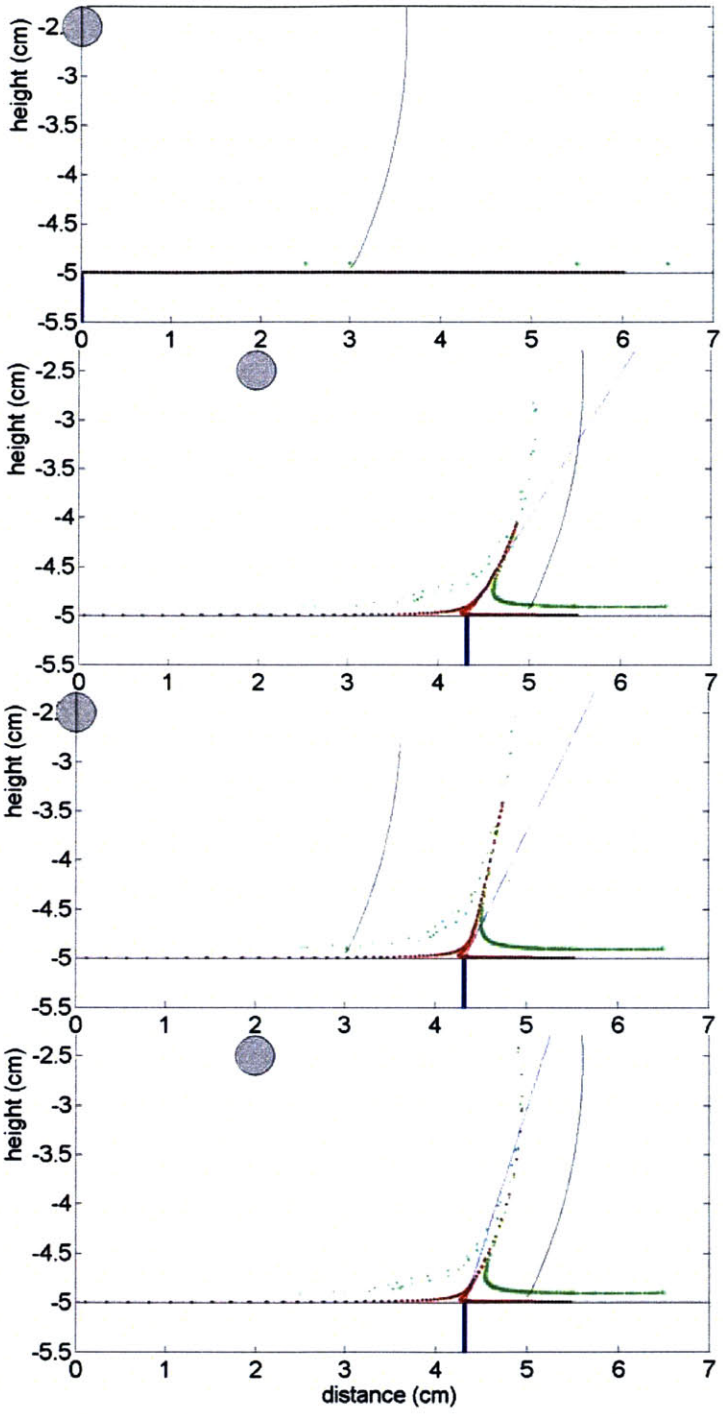

Figure 5-3: Periodic flow with peak-to-peak amplitude $A = 2$ cm and frequency $\alpha = 5$ rad/sec. Streak lines are illustrated in green, material lines in red, and instantaneous zero skin friction streamline in black. Haller's criteria is in blue and uses a first order approximation for the separation profile slope.

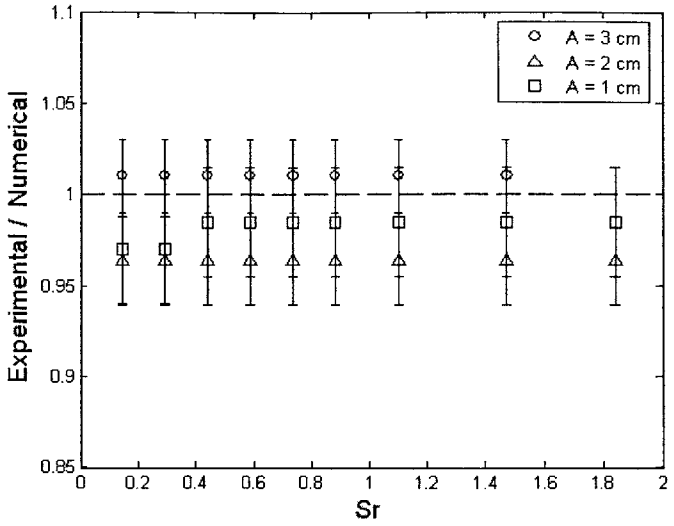

Figure 5-4: Comparison of the experimental results obtained by flow visualization and numerical simulation for the separation point in a time-periodic flow using criterion given by equation (1.1).

To compare the location of separation in the experiments with the numerical models, the flow simulations were performed utilizing the same Re and Sr for the experimental results shown in figure 5-2. The criteria developed by Haller used as input the shear stress data generated from the FLUENT model. Figure 5-4 summarizes the results. There is a close agreement between the experimental visualizations and the results from Haller theory, with agreement being typically better than 5 % over the range of Strouhal numbers investigated

A direct comparison between streak lines visualized in an experiment and a numeric simulation is shown in figure 5-5. The parameters for simulation were peak-to-peak amplitude $A = 3$ cm, oscillatory frequency $\alpha = 2$ rad/sec, and distance of the cylinder from the wall $c =$ 2.5 cm. The numerical and experimental images are taken at same times. The blue lines in the pictures indicate the separation point and separation profile obtained via equations (5.4) and (5.5), utilizing shear stress and pressure generated numerically. Figure 5-5 shows that the quasi-steady approximation for the rotor-oscillator flow is valid for time periodic flows at low Re and Sr numbers, as in the vicinity of the wall, numerics and dye visualization revealed that fixed separation occurs at the same location within ± 1 mm. Dye visualization shows that as

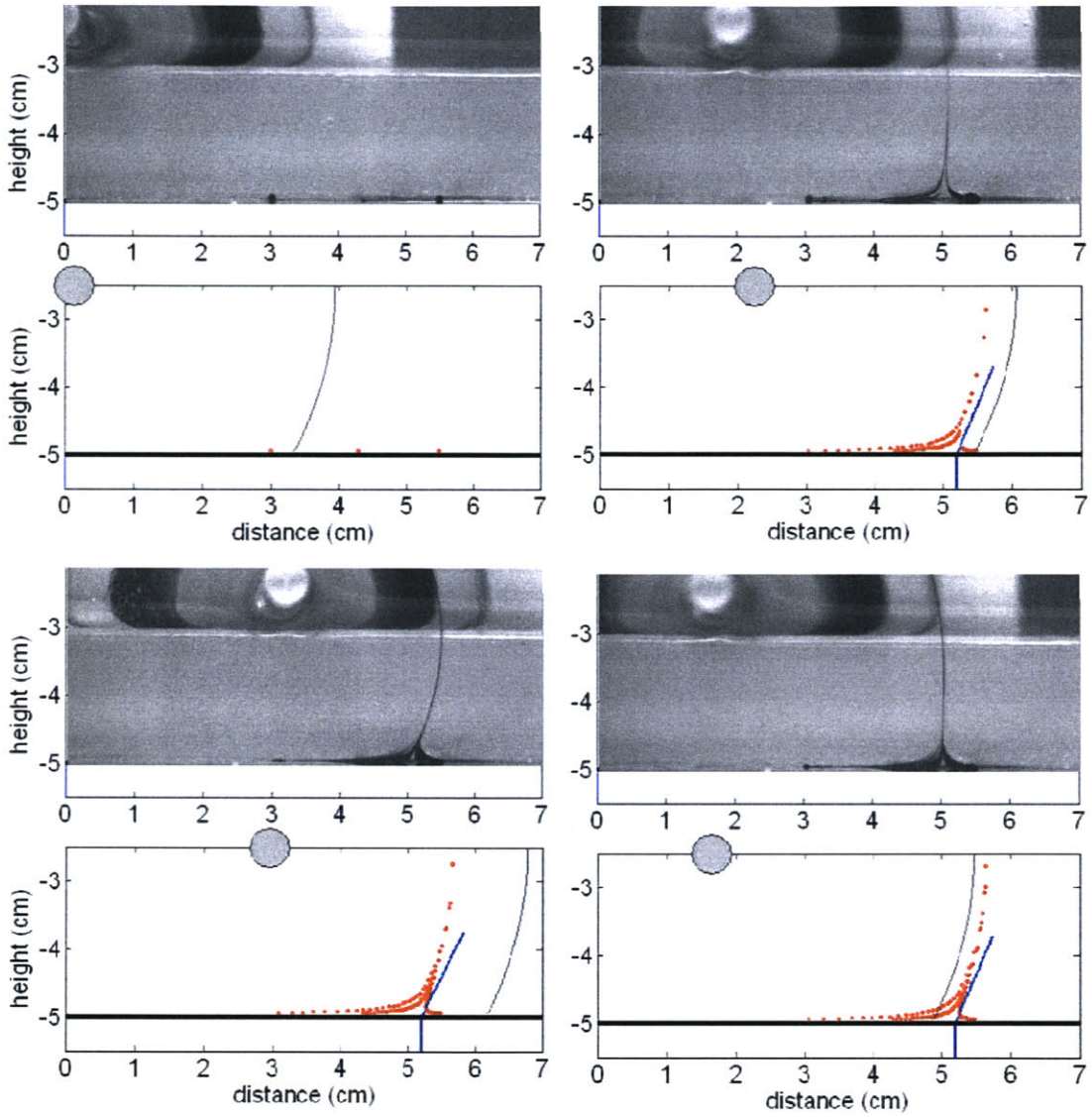

Figure 5-5: Fixed separation in periodic flow. The peak-to-peak amplitude of oscillation A = 3 cm, the frequency α = 2 rad/sec. The comparison between visualization and numerical simulations is displayed. As time advances, the separation point remains fixed. Time advances from left to right and top to bottom.

the cylinder reaches the origin of its oscillation the separation profile becomes steeper in the experiment, this behavior is not captured by the numerics. However, as the cylinder reaches the far end of its oscillation, the separation profile from numerics and visualization are qualitatively similar. The difference in shape of the separation profile could be attributed to inertia effects neglected in the simulations or three-dimensional effects in the dye visualizations.

5.3 Fixed separation in aperiodic flows

In the theory developed by Haller, the existence of fixed separation points is not limited to periodic flows, but extends to aperiodic flows that contain a unique zero-mean skin friction point as time progresses [10]. To investigate this in the rotor-oscillator flow, an aperiodic flow was introduced using a random translational motion for the cylinder along the long axis of the tank. Numerical simulation and experiments in this work demonstrate that fixed separation can be encountered in aperiodic flows as predicted by Haller [10].

5.3.1 Experimental results

The random motion imposed along the translational axis of the cylinder was generated using the commercial package LabVIEW. In order to generate the random motion, a number between -1 and +1 was chosen with equal probability, and multiplied by half the maximum peak-to-peak amplitude, resulting in a new position of the cylinder relative to the origin (the position of the cylinder at time $t = 0$). The cylinder then made a move from its original position to the newly assigned location. In this way, the translational motion had a zero mean displacement due that the back and forth random cylinder motion around origin. All cylinder moves had the same duration, therefore each move had a different velocity since the new cylinder location was generated at random. In figure 5-6 a typical position profile of the cylinder translation along the tank is presented.

The main variable adjusted in the experiments was the maximum amplitude for the cylinder translation. As in the periodic experiments, the distance of the cylinder from the wall was kept constant at $c = 2.5$ cm and the angular velocity at $\omega = 60$ rad/sec. The different peak-to-peak amplitudes for the cylinder translation ranged between 1 cm and 3 cm. Because each

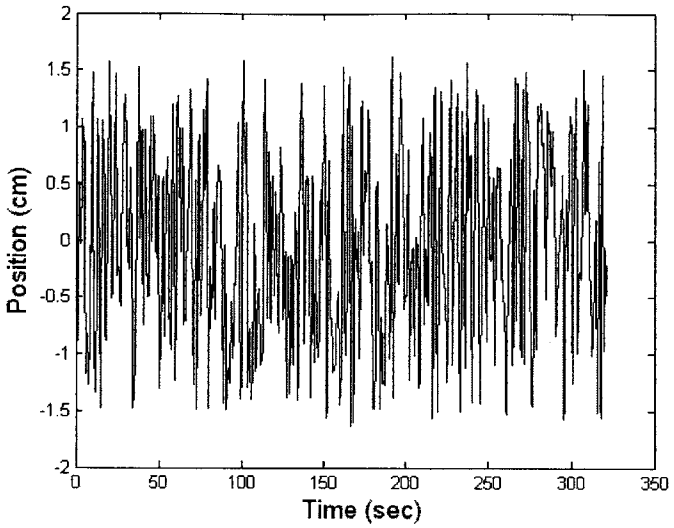

Figure 5-6: Position of the cylinder as a function of time. The signal is random and possesses a zero mean, its maximum peak-to-peak amplitude is 3 cm.

experiment was generated with a distinct random pattern, experiments were repeated three times for each translational amplitude to ensure that the separation point was not dependent on the nature of the random motion. The location of the separation point was recorded utilizing dye visualization, with a characteristic error of ± 1 mm due to the finite width of the dye line. The typical duration of each run was approximately 2 minutes, long enough to remove the transients and observe fixed separation.

The data points collected from the experiments are shown in figure 5-7. As the amplitude of the tests was increased, the location of fixed separation moved away from the origin, as observed in the time-periodic experiments. Although each of the three experiments performed with the same amplitude utilized a different random sequence, the location of the separation point was the same and remained fixed over the time span of the experiments. The experimental results indicate that the random forcing results in a unique point of zero skin friction at the boundary wall, and this is the point where separation occurs.

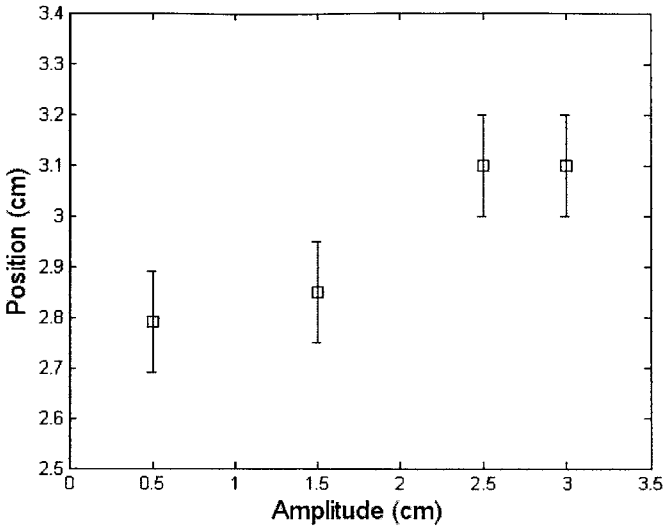

Figure 5-7: Experimental results for separation point in a flow field with random forcing. Each data point is the average of three experimental measurements.

5.3.2 Comparison of flow visualization experiments with numerical simulations

Because of the small Re and Sr, a quasi-steady approximation was applied. In this flow the Re is defined as in equation (2.5), the Sr is defined as

$$Sr = \frac{c^2}{r^2 \omega \tau} \tag{5.13}$$

where c is the distance of the cylinder to the wall, r is the radius of the cylinder, ω is the angular velocity, and τ is the typical time scale for the cylinder random translation. A typical value for τ is 2 sec, thus the Sr is of the order of unity showing that the quasi-steady approximation still can produce meaningful results. Using numerical simulation, the point of separation was determined by applying Haller's criteria, using as input the numerical shear stress generated in FLUENT. The comparison between the experimental measurements of the separation point under random forcing with different amplitudes and the separation points determined using Haller's criteria is presented in figure 5-8. Both measurements differed in less than 2 %.

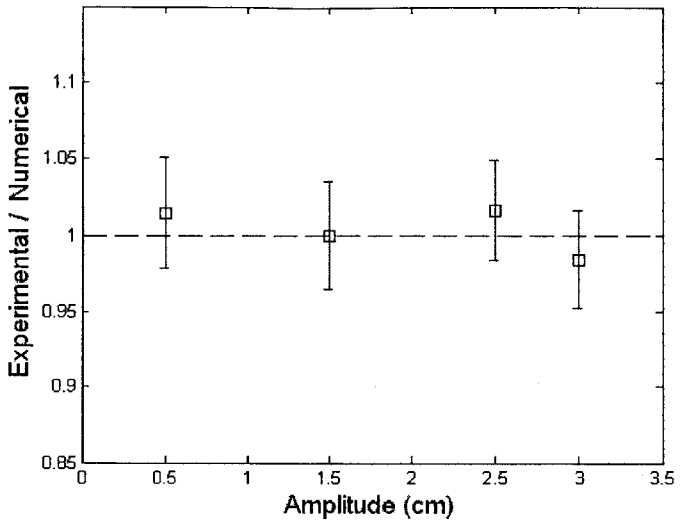

Figure 5-8: Comparison between separation point measured by dye visualization and its predicted value employing Haller's criteria applied on FLUENT generated shear stress.

Particle tracking in the flow field under a random forcing was obtained using the quasi-steady approximation for the rotor-oscillator solution developed by Hackborn [6]. In similar fashion to the periodic flow solution, it was assumed that as the cylinder translates the inertia effects are negligible, and at every time step the flow field is a replica of the field at a previous time. Mathematically, the flow solution is translated with the equation

$$y = y_0 - r(t) \tag{5.14}$$

where y is the long axis of the tank, y_0 is the initial position, and $r(t)$ is the random motion term.

Figure 5-9 shows a comparison between the experimental material line dye visualization and numerical material line simulation obtained utilizing Hackborn's solution. The blue line in the experimental pictures uses Haller criteria with shear stress and pressure generated by the FLUENT model; the instantaneous zero skin friction streamline is shown in black. Haller's criteria accurately captures the point of fixed separation. In the same manner as the periodic flows the separation profile is time dependent, the first order approximation is shown in figure

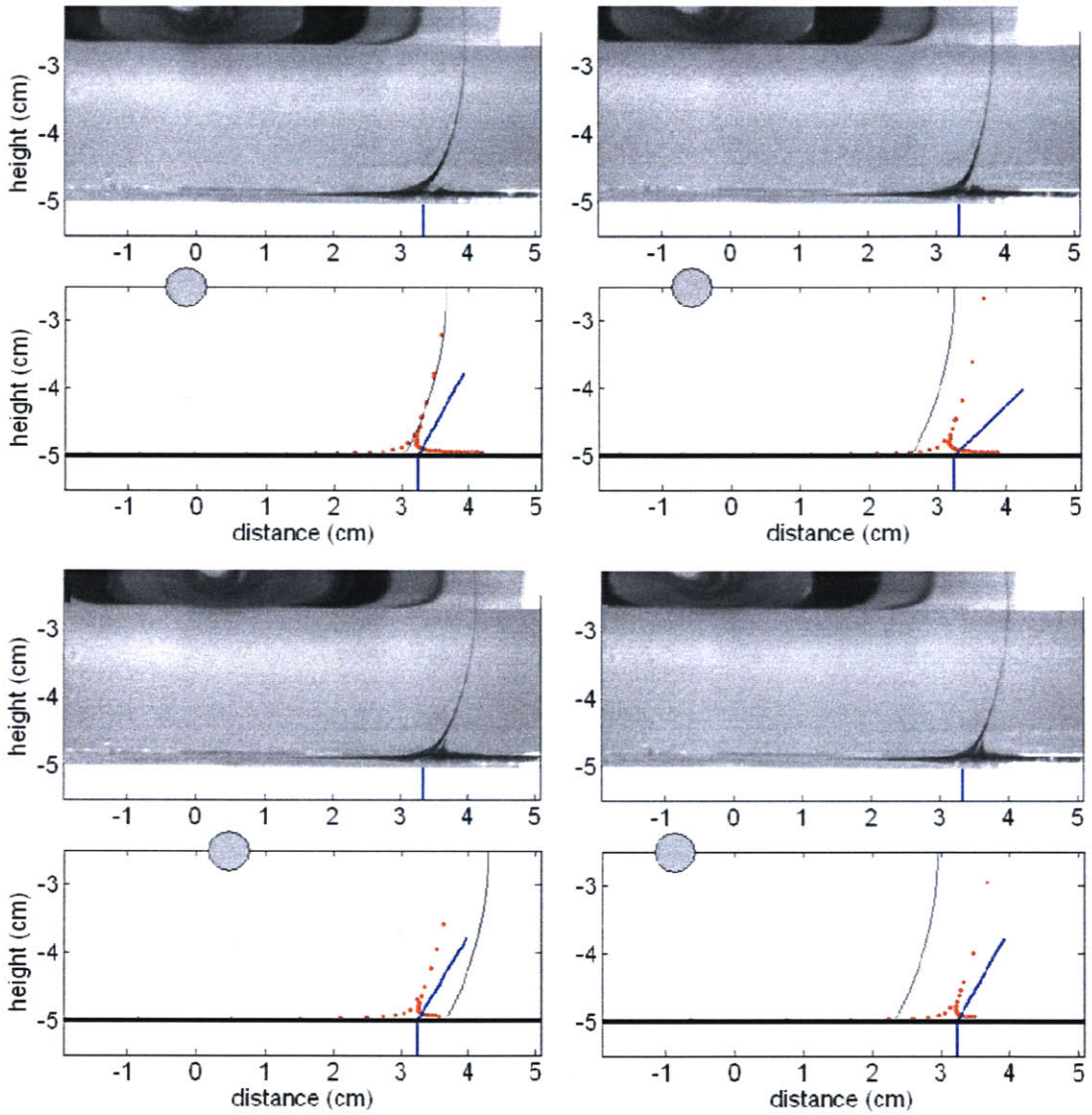

Figure 5-9: Fixed separation in random flow. The maximum peak-to-peak amplitude $A = 2$ cm. The dye visualization and numerical simulation indicate fixed flow separation in a random flow with zero mean displacement.

5-9. The predicted separation profile is slightly flatter than the profile drawn by the dye. Simulation indicates that the instantaneous zero skin friction streamline position changes in similar fashion as the position of the cylinder, yet separation takes place in a fixed position strengthening the notion that in unsteady flow the time history of the shear stress determines flow separation.

Chapter 6

Moving separation in unsteady flows

In chapter 5 fixed separation in unsteady flow was investigated. Particularly, fixed separation points were encountered in periodic flows with frequencies of oscillation $\alpha = 0.1$ rad/sec or higher. Additionally, a flow field generated by a random motion of the cylinder was considered. The flow admitted a location on the wall where the mean skin friction was zero at all times, resulting in fixed separation.

In the limit of infinitesimally small frequency for a periodic flow, the oscillatory time scale becomes dramatically larger than the time scale at which flow ejection from the wall occurs, suggesting that the separation point could move along the boundary. In the case of the random flow experiments, the random motion of the cylinder could be superimposed on a slow drift in one direction, in which case there would not be a point on the wall with zero mean skin friction for all times, hence, fixed separation would not occur. In this scenario too, the separation structure could move along the wall, following the slow drift. The work presented in the current chapter investigates the existence of separation points that move along the boundary wall, focusing on simulations and dye visualizations of a slow periodic flow and random flow with a linear drift.

6.1 Theoretical treatment of moving separation

As discussed in chapter 1, in moving separation the separation point moves as time advances. Associated with the moving separation point is a moving separation profile that is modeled

using a finite time invariant manifold [9] [10]. The criteria developed by Haller determines the separation point γ at a time t_0 using the following equations

$$\gamma(t_0) = \frac{1}{2}[\gamma_+(t_0 - T_m(t_0), t_0) + \gamma_-(t_0 - T_m(t_0), t_0)], \tag{6.1}$$

where γ_+ and γ_- are effective separation points obtained from

$$\int_{t_0}^{t} \frac{u_y(\gamma_{eff}, 0, \tau)}{\rho(\gamma_{eff}, 0, \tau)} d\tau = 0, \tag{6.2}$$

for the time intervals

$$\gamma_+(t, t_0) = \sup_{s \in [t, t_0)} \gamma_{eff}(s, t_0), \qquad \gamma_-(t, t_0) = \inf_{s \in [t, t_0)} \gamma_{eff}(s, t_0), \tag{6.3}$$

and T_m is a time scale defined later. Then, the spatial interval containing the separation point is

$$\delta(t, t_0) = \gamma_+(t, t_0) - \gamma_-(t, t_0) \tag{6.4}$$

which must satisfy the condition

$$\frac{1}{2}\delta(t_0 - T_m(t_0), t_0) \int_{t_0 - T_m(t_0)}^{t_0} \max_{x \in I(t_0 - T_m(t_0), t_0)} |u_{xy}(x, 0, t)| dt = 1, \tag{6.5}$$

$$\max_{x \in I(t_0 - T_m(t_0), t_0)} u_{xy}(x, 0, t) < 0, \qquad t \in [t_0 - T_m(t_0), t_0], \tag{6.6}$$

where $T_m(t_0)$ is the time scale that distinguishes the unstable manifold that remains close to the separation point for the longest time. The slope of the separation profile is determined via

$$f_0(t_0) = \frac{\int_{t_0}^{t_0 - T_m(t_0)} \left[u_{yy}(\gamma_{eff}, 0, \tau) + 3u_{xy}(\gamma_{eff}, 0, \tau) \int_{t_0}^{\tau} u_y(\gamma_{eff}, 0, s) ds \right] d\tau}{3 \int_{t_0}^{t_0 - T_m(t_0)} u_{xy}(\gamma_{eff}, 0, \tau) d\tau}. \tag{6.7}$$

6.2 Moving separation in slow periodic flow

The experiments in this section concern separation in a low frequency oscillatory flow. Experiments were performed at a frequency $\alpha = 0.01$ rad/sec and both flow visualization and shear stress measurements were taken. In order to visualize the location of separation, streak lines

were initialized at the boundary wall. The experimental results were supported by numerical simulations, utilizing Hackborn's analytic solution to model the dye visualization and FLUENT to compare the shear stress measurements.

Images of the slow oscillatory flow are shown in figure 6-1. A peak-to-peak amplitude $A = 3$ cm, separation of the cylinder from the wall $c = 2.5$ cm, and angular velocity $\omega = 60$ rad/sec were considered. A quasi-steady approximation for the Hackborn solution was utilized to simulate the flow field and separation criteria given by equations (6.1) through (6.7) were applied to the numeric simulations. The separation point and slope calculated using Haller's criteria are indicated in blue while the instantaneous zero skin friction streamline is shown in black. The oscillatory motion starts in frame 6-1(a) with the cylinder moving towards the right. In frame 6-1(b) the cylinder reaches one end of the oscillation and starts its journey back to finish in frame 6-1(d). As time advances, the separation location moves along with the cylinder. Haller's criteria follows the zero skin friction point closely, however the numerical visualizations indicate that the point where the streak lines are ejected differs on the order of 1 mm from the moving separation criteria. Although this is a periodic flow and in theory we have fixed separation, for practical purposes, the observed point of separation is moving.

In addition to the visualizations, shear stress measurements were taken during the slow oscillatory motion. The shear stress measurements were acquired utilizing one hot wire, whose calibration procedure is described in chapter 3. As discussed in section 3.2, the time response of the sensing element allows taking measurements in periodic flows with small oscillatory frequency α, but not for large values of α. In figure 6-2 the time dependent shear stress at a fixed position in the wall is shown. The time dependent experimental shear measurements showed agreement to better than 15% when compared to numerical simulations.

We applied Haller's criteria to both the anemometer shear stress measurements as well as to FLUENT generated shear profiles. In figure 6-3 a comparison between numerical and experimental prediction of the separation point is shown. Experimental shear stress and numerical shear stress resulted in moving separation points that were on the order of 1 mm apart.

In addition to the shear measurements, the dye visualization allowed direct measurement of the separation point with an accuracy of 1.5 mm because of the finite width of the separation profile. In figure 6-4 a comparison between the position of the zero skin friction point and the

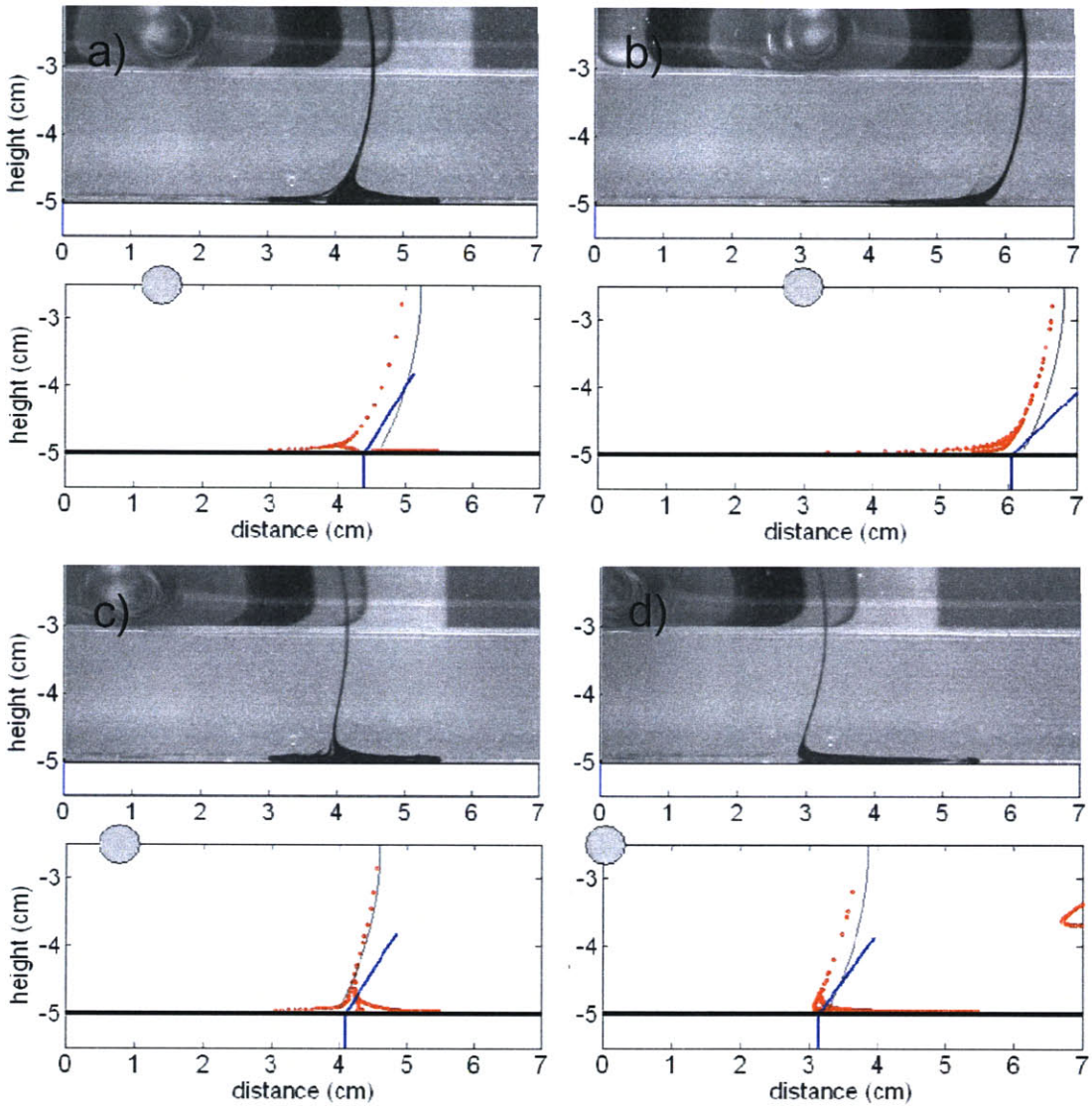

Figure 6-1: Comparison between numeric and dye visualization of slow oscillatory flow. The frequency $\alpha = 0.01$ rad/sec, and the amplitude of oscillation is $A = 1.5$ cm. The numerical simulations utilized the Hackborn solution.

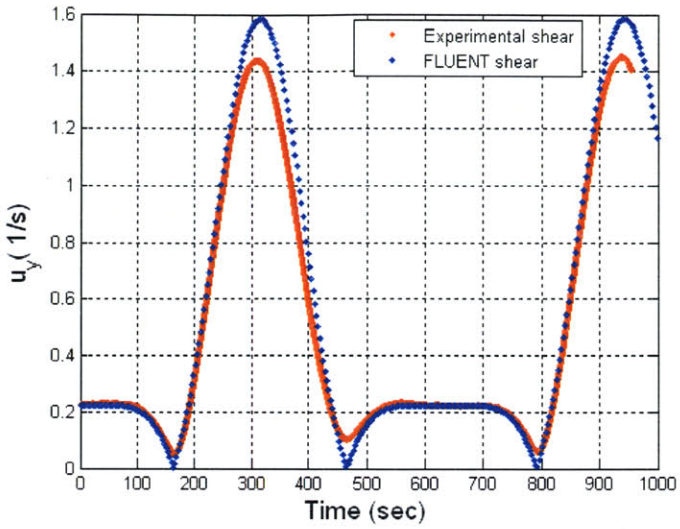

Figure 6-2: Time dependent shear stress experimentally measured and computed utilizing FLUENT.

location of flow separation determined from shear measurements and dye visualization is shown. The moving separation point determined from experimental shear stress via Haller criteria and the dye visualizations closely follow the zero skin friction point. The experimental measurements differ from the zero skin friction point by 1.5 mm. Constraints such as sensor resolution and finite width of the dye do not allow better accuracy in the results. At the beginning of the flow motion, Haller's criteria does not possess enough information to determine the point of separation, as indicated in figure 6-5. Conditions (6.1) through (6.6) fail to be satisfied due to the lack of information regarding the flow dynamics. Because the shear stress values measured with sensors differ from those simulated by FLUENT, the time at which the first separation point can be computed is not the same for both methods. This is also illustrated in figure 6-5.

In chapter 5 identical parameters were used for the periodic flows studied, however, a larger frequency for oscillation resulted in fixed separation. Thus, visualizations suggest that there is a transition from fixed separation to moving separation as the oscillatory frequency is reduced. Specifically, if the frequency of the oscillatory motion is incrementally reduced, the time scale at which fluid is ejected from the wall becomes more important than the time scale of unsteadiness

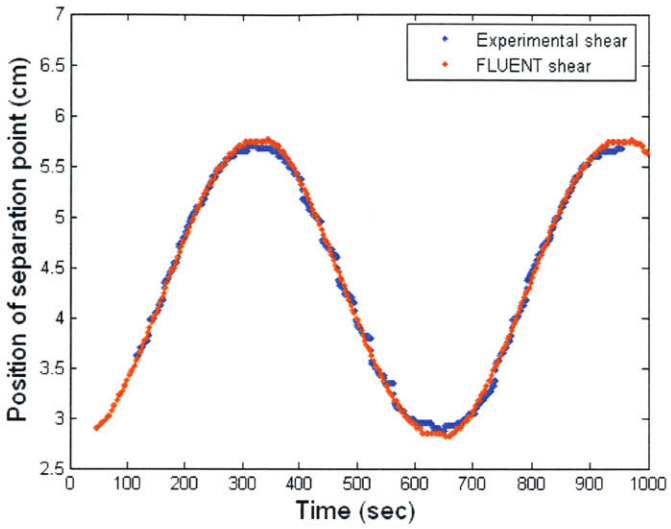

Figure 6-3: Moving separation point computed from shear stress sensor and FLUENT shear field via Haller's criteria.

or period of oscillation. In theory, the criteria for fixed separation still applies for the slow oscillatory motion; however, as α goes to zero the resulting unstable manifold aligns closer to the wall, implying that if the dye were infinitely thin, it could be possible to distinguish a fixed separation point. In practice, on the length scales we are considering, the point of separation moves along the boundary wall. Thus, Haller's moving separation criteria is better suited for capturing the physical phenomena.

6.3 Moving separation in aperiodic flows

In the previous section moving separation in a slow periodic flow was discussed. The results showed that the separation point closely followed the zero skin friction point in a slow periodic flow. In this section, moving separation in an aperiodic flow is investigated by means of numerical simulation and dye visualization. More specifically, the flow field resulting from a random fluctuation imposed over a linear translation of the cylinder is considered.

The type of translational motion and the rotational rate of the cylinder determine the nature of flow separation on the boundary wall. Previous results indicated that the flow field

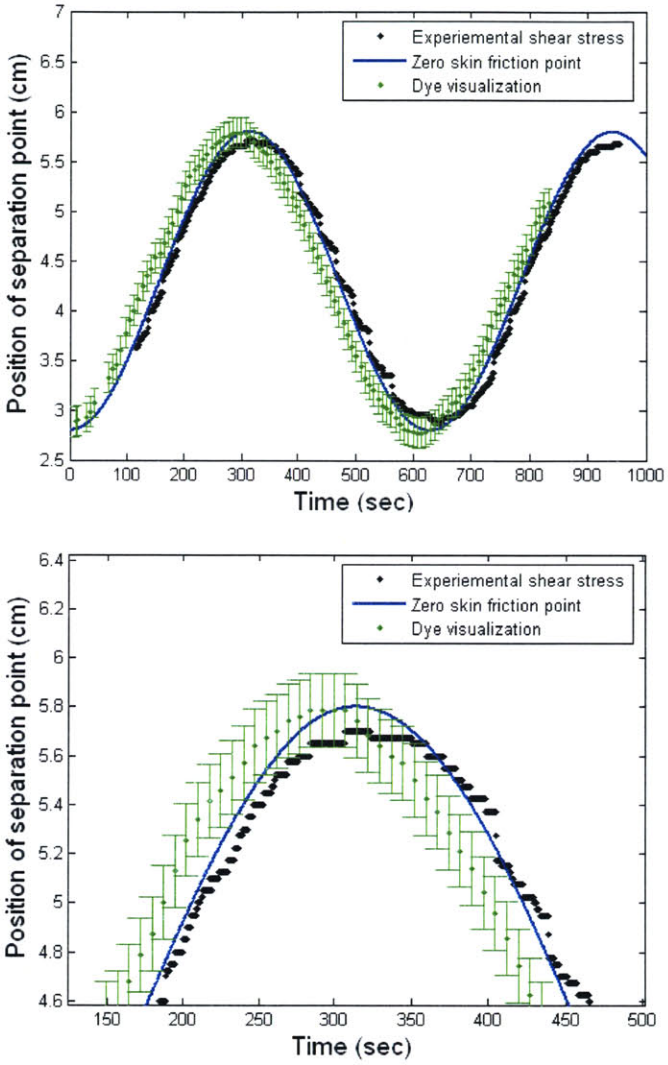

Figure 6-4: Separation point measured from dye visualization and from shear measurements compared to the position of the zero skin friction point.

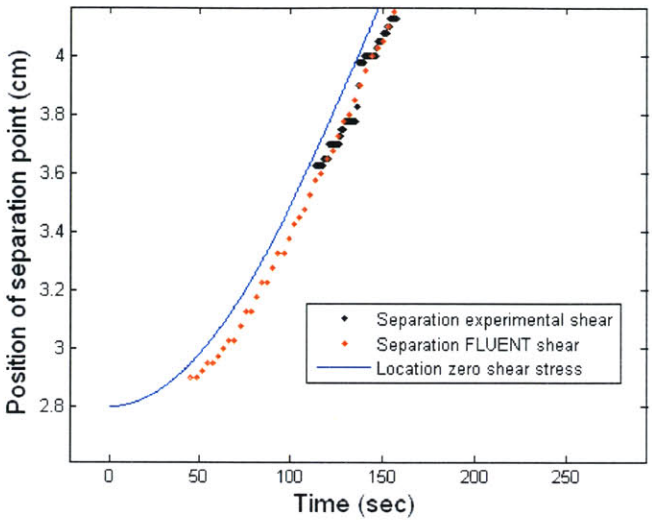

Figure 6-5: Onset of flow motion provides insufficient information to utilize moving separation criteria.

generated by a purely random translational motion of the cylinder induces a fixed separation point. This result is expected, since the translational motion had a zero-mean displacement that also resulted in a zero-mean skin friction point for all times. In the present study, however, the random motion of the cylinder is superimposed on a linear drift, producing a non-zero mean skin friction point and hence moving separation. The type of translational motion used by the cylinder to induce moving separation is illustrated in figure 6-6.

By means of dye visualization, the random flow plus linear drift was observed in the rotor-oscillator flow. Random fluctuations in the motion were introduced every 2 seconds, and the linear drift had a rate of 0.0625 cm/sec. Dye visualization showed that the separation point moved along the wall, following the slow linear drift of the cylinder. The random fluctuations had almost no effect in the position of the separation point. In figure 6-7 images of the separation profile are shown. The motion of the cylinder lasts approximately 90 seconds. Each image is taken at nearly 30 seconds intervals. In frame 6-7(a) the cylinder has moved from the origin for 30 seconds, approximately 30 seconds later the cylinder is in frame 6-7(b), finally the cylinder stops its motion in frame 6-7(c). The separation point moved seemingly equal distances at each

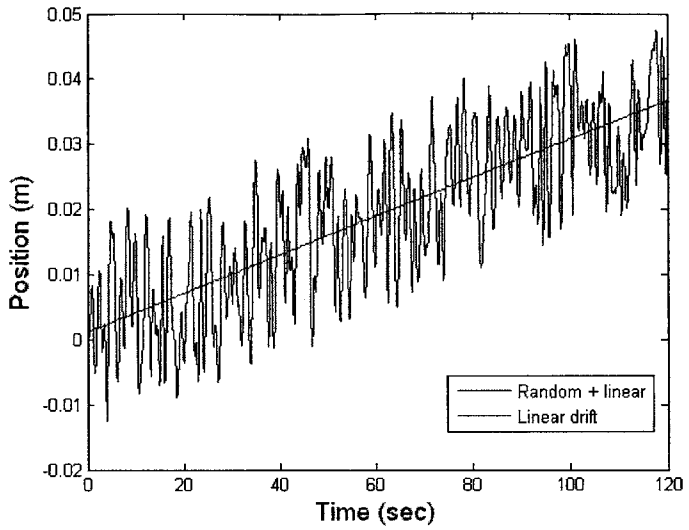

Figure 6-6: Motion of the cylinder as time advances. The trajectory is generated by adding a random signal of zero mean and a linear profile.

frame, suggesting that the linear drift was determining the motion of the separation point.

Building upon observation of the dye visualization we investigated separation numerically, adopting a quasi-steady approximation of the flow field. In similar fashion to chapter 5, the shear profile was obtained using FLUENT commercial software. The quasi-steady approximation for the time dependence results in the instantaneous zero-skin friction streamline moving in the same manner as the cylinder driving the flow.

There were three important time scales to consider in this arrangement: the linear drift time scale, the random time scale, and the rate of rotation of the cylinder. The first two time scales relate to the unsteadiness, and the latter relates to the ejection rate. In similar fashion to the slow periodic flow, a slow linear motion will result in the location of separation closely following the zero skin friction point. However, if random perturbations are introduced, it is expected that the zero skin friction point will fluctuate significantly about the separation point.

Initially, if we consider random fluctuations occurring on a time scale comparable to that of the linear drift, it is expected that separation closely follows the zero skin friction point. This behavior is illustrated in figure 6-8. The random perturbations were introduced every 5 seconds,

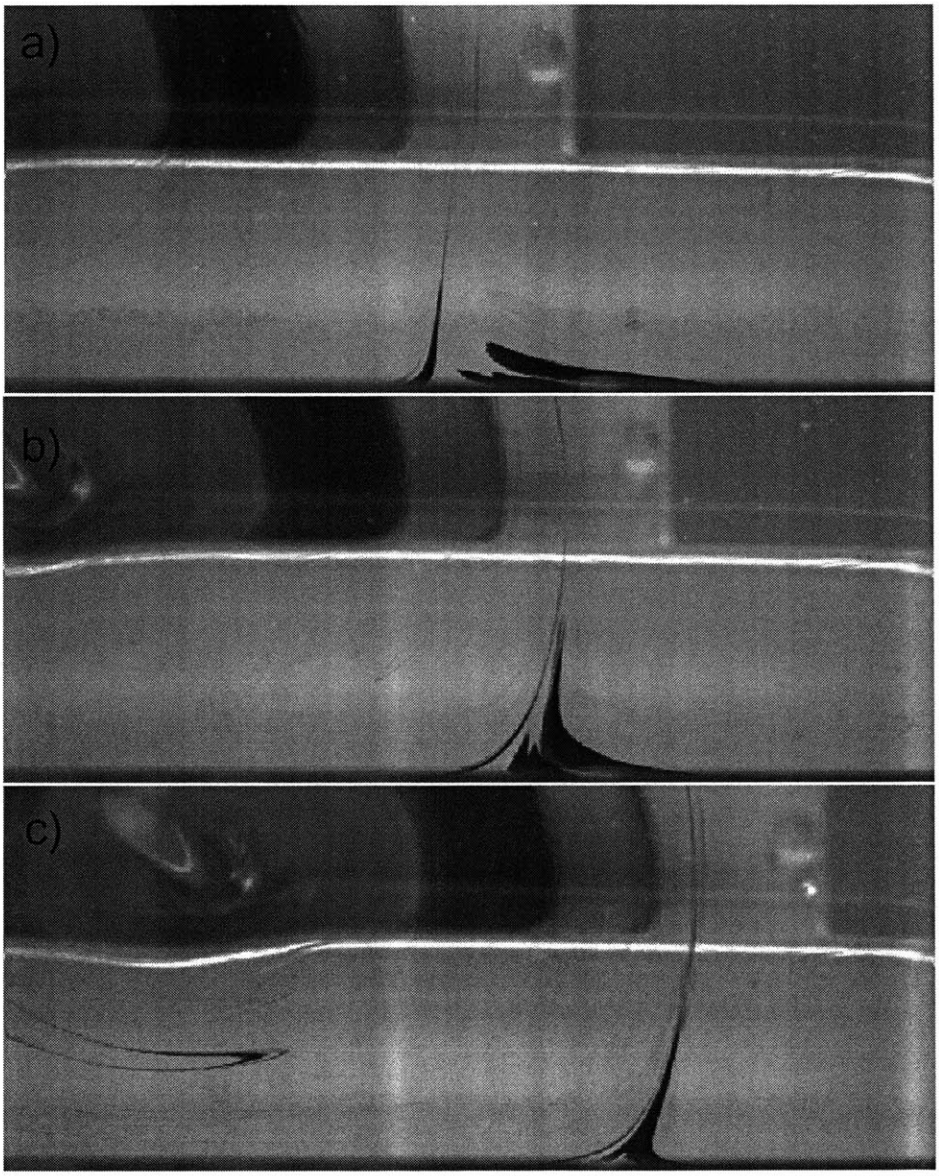

Figure 6-7: Flow separation in a random flow with linear drift. The separation of the cylinder from the wall $c = 2.5$ cm.

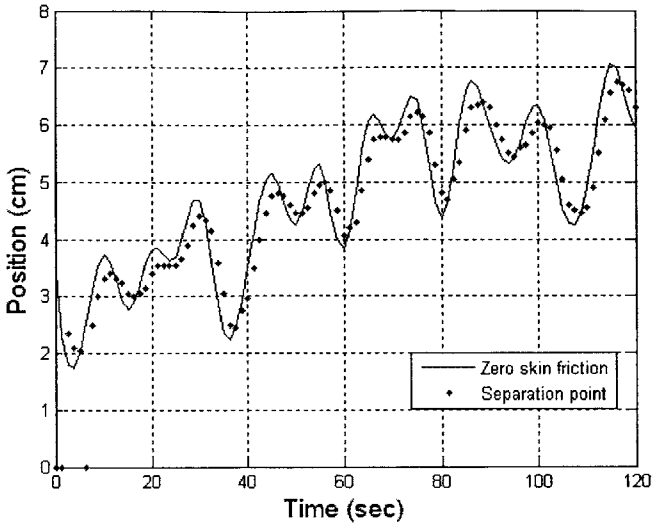

Figure 6-8: Moving separation in flow driven by random fluctuation over a linear drift. The random perturbations are introduced every 5 seconds.

and had a maximum peak-to-peak amplitude of 1.5 cm. Utilizing the moving separation criteria given by equation (6.1) through (6.6), the location for flow separation was shown to follow closely the zero skin friction point. As the frequency of random perturbations increased, the separation point started to distance itself from the zero skin friction point. In figure 6-9 the separation point in a flow field with random perturbations occurring at a higher frequency is shown. The random fluctuations occurred every 0.1 seconds and the maximum amplitude was again 1.5 cm. As expected, the motion of the separation point receded from the zero skin friction point. In figure 6-10 a closer view of moving separation is shown. The average displacement of the moving separation point in figure 6-9 is 3.6 mm, differing significantly from the results obtained for low frequency random oscillation shown in figure 6-8 where the average displacement of the separation point is 5.6 mm.

In order to illustrate the effect of the time scale of the random perturbations, a study of the separation point under random fluctuations introduced at different time scales was performed. For all the simulations, the maximum displacement of the random motion was 1.5 cm. In figure 6-11 the results are presented. On the y axis the mean displacement of the separation point is

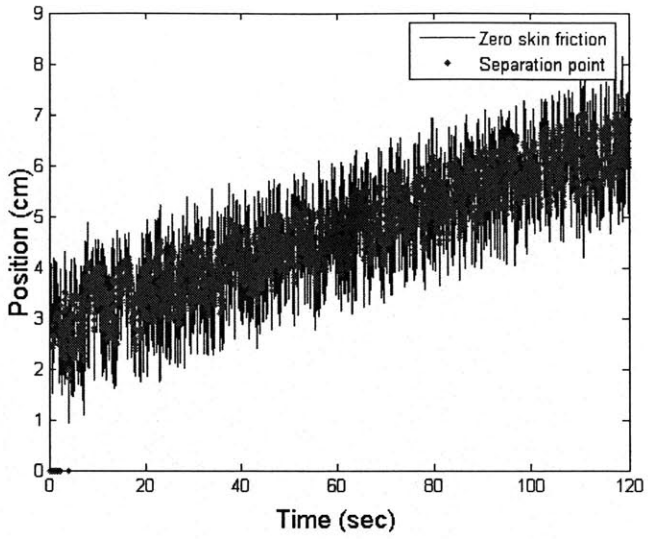

Figure 6-9: Moving separation in flow driven by random fluctuation over linear drift. The random perturbations are introduced every 0.1 seconds.

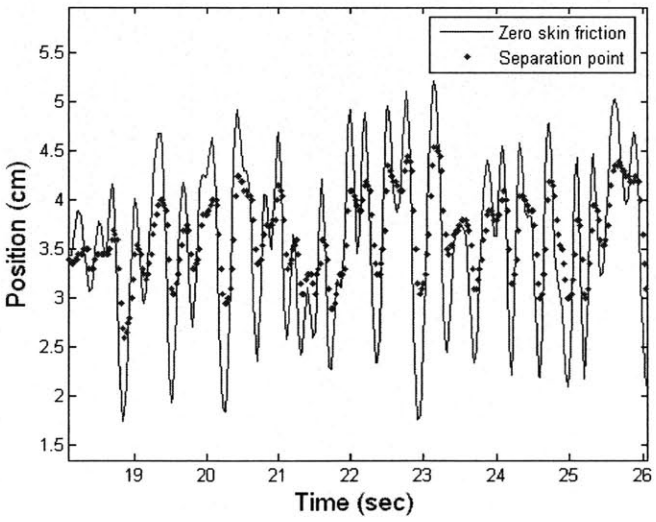

Figure 6-10: Closer look at the separation point in the random+linear driven flow.

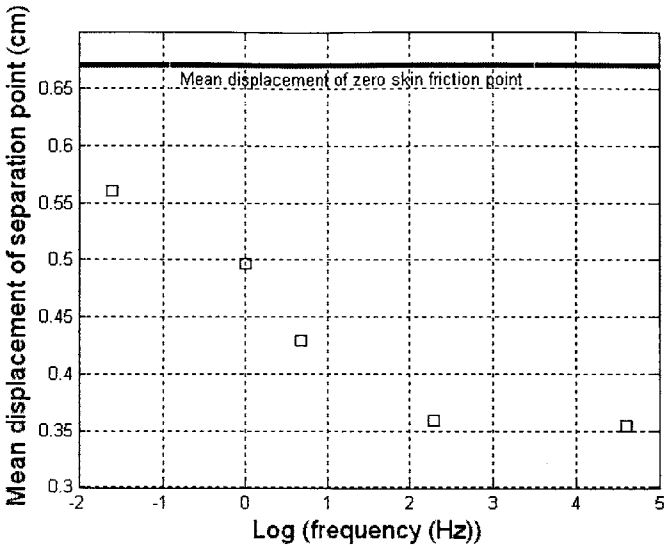

Figure 6-11: Mean displacement of the separation point for random fluctuations introduced at different time scales.

shown and the mean displacement of the zero skin friction point is 6.7 mm. As the time scale for the random fluctuations was made smaller the moving separation point did not follow the zero skin friction point as closely. The simulations started with random fluctuations entering at a frequency of 0.2 Hz resulting in a separation point mean displacement of 5.6 mm; increasing the frequency to 100 Hz damped the mean displacement of the separation point to 3.6 mm as shown in figure 6-11.

As the frequency was increased, the Sr number became larger and inertial effects became important so that a Navier-Stokes solution is necessary to obtain accurate results in the simulations. The numerical simulations employed Sr between 0.2 and 110. In figure 6-11 the points corresponding to a mean displacement of 0.36 cm and 0.35 cm correspond to a Sr of 11 and 110 respectively, breaking the quasi-steady approximation.

The flows investigated in this chapter show moving separation structures along the wall. The slow oscillatory motion in theory admits a zero mean skin friction point as time goes to infinity, but in practice it has been shown that the separation structure can be accurately followed using the moving separation criteria. In the case of the random flow plus linear drift,

it was demonstrated that in the limit where the random fluctuations occur at very small time scales compared to the time scale of the linear drift, the moving separation point tends to follow the underlying linear motion of the cylinder. On the other hand, if the both time scales are comparable, the separation point follows closely the instantaneous zero skin friction point.

Chapter 7

Conclusions

Unsteady separation has been an outstanding issue that has received attention from theoreticians as well as experimentalists over the last century. Nevertheless, a precise definition and thorough understanding of separation in unsteady flow is still a source of debate. In the present work, we have embraced a Lagrangian approach to fluid separation and have investigated the recently developed theory by Haller [10]. Specifically, separation experiments and numerical simulation were performed using the so-called rotor-oscillator flow [8]. Flow visualization and shear stress measurements were acquired through the experiments, whilst numerical simulations were utilized to corroborate the experimental observations. In the following paragraphs a summary of the findings of this research is presented.

The experimental investigations verified the existence of well defined separation structures in unsteady flow. More specifically, fixed separation points and moving separation points in a viscous flow with different types of time dependence were encountered, as predicted in Haller's theory [10]. The separation criteria successfully captured the trend of the separation structures, demonstrating that fluid separation in unsteady flow can be better comprehended from a Lagrangian perspective. In addition, the notion of weighting the shear stress, rather than looking to the instantaneous zero skin friction alone to determine separation, was emphasized in experiments containing fixed and moving separation structures.

Fixed separation, this being separation that originates at a fixed point on the boundary, was investigated in flow fields with two types of time dependence: periodic and random. In both type of flows, the existence of a unique stationary point where flow ejection occurs at

all times was verified employing dye visualization and numerical simulation. Experimentally, dye visualization of the flow allowed direct measurement of the separation point. In order to find the separation point, streak lines were placed at the wall vicinity and the point of separation was measured with an accuracy of ± 1 mm. The rotor-oscillator experiments in the time-periodic flow indicated that for a fixed amplitude of oscillation the location of the fixed separation point is independent of the frequency of oscillation, provided that the frequency does not approach to zero. By assuming a quasi-steady behavior of the flow field, streak lines were simulated for the time-periodic experiments. Additionally, the shear stress profile on the wall was simulated to apply Haller's fixed separation and determine the separation point. The location of the separation point in the periodic flow based on streak line visualization, experimental or numerical, agreed with the predicted value by Haller's criteria within 4 %.

The theory developed by Haller demonstrates that a flow field containing a point on the boundary with vanishing mean skin friction for all time admits a fixed separation point. Therefore, fixed separation is not limited to periodic flows, or a flow with a well defined time dependence. Indeed, the theory predicts that fixed separation can occur for random motion with zero-mean displacement in the rotor-oscillator flow. In a similar manner to the investigations in periodic flows, the location of the separation point was determined via dye visualization and numerical simulation for a random flow. Physically flow separation was observable using either streak or material lines: the former was utilized in the periodic flow studies while the latter was implemented in the random flow. By means of a quasi-steady approximation of the flow field, the shear stress was simulated and Haller's criteria for fixed separation was applied to the data. The predictions utilizing the fixed separation criteria agreed closely with the experimental observations, typically to within 4 % accuracy.

A separation structure that moves along the wall as time progresses is termed moving separation. This type of separation was investigated in two environments: in a slow periodic flow field, and in a random flow field with slow translational drift. The periodic flow was characterized by its highly quasi-steady behavior, due to its small frequency of oscillation. In this scenario, Haller's criteria for moving separation was applied to both numerically-generated and experimentally-measured shear stress. In the case of the experimentally measured shear, a hot wire anemometer was placed in the wall and utilized to obtain time-dependent measurements.

The numerical simulation followed the quasi-steady approach from the fixed separation studies. Thus, moving separation was determined with both techniques and the resulting locations for fluid separation agreed within ± 1 mm. The position of the separation point via Haller's criteria differed by less than 5% from the observed separation, demonstrating accuracy and feasibility of the method.

Continuing the study of moving separation, we then considered a flow field that does not contain a particular location on the wall where the mean skin friction vanishes for all times. For this flow the motion of the cylinder comprised random motion plus linear drift. This flow field was investigated predominantly by numerical simulation, although supporting experimental visualizations were performed. In order to perform the numerics, random motion with Sr between 0.2 and 110 were considered. By generating the shear stress numerically, Haller's criteria was applied to random motions with increasing Sr and a fixed amplitude of oscillation. Basic flow visualization was undertaken to qualitatively understand the nature of the moving separation point. As expected, for a cylinder motion where the random fluctuations occur at small time scales compared to the linear drift, the separation point moves along the wall at a similar rate as the linear drift. The general trend showed that as the random fluctuations occurred on shorter time scales, they became less important and the separation point followed the linear drift more closely. As the time scale of the random fluctuations approached zero, the experience obtained from flow visualization suggests that there should be nearly no fluctuation of the separation point around the linear drift motion. However, the random component of the moving separation points in the numerical simulations were not fully damped, disagreeing with the experimental observations.

The investigations demonstrated that unsteady flows admit points of separation that can remain stationary or move along a wall, depending on the flow conditions. What is more, experimental observations indicated that there are length scales and time scales that determine whether we perceive separation as fixed or moving. Specifically, in the rotor-oscillator experiment there are two important length scales: the unsteadiness length scale, x_u, and the ejection length scale x_e. The first length scale comes from the motion of the zero skin friction point along the wall, which is determined by the translational motion of the cylinder in this study, whilst the second length scale is determined by the distance from the wall at which the sepa-

ration structure encounters the main flow field; for example, in a boundary layer the ejection length scale is the boundary layer thickness. Additionally, there are two important time scales: the unsteadiness time scale, t_u, and the ejection time scale, t_e. In the rotor-oscillator flow the unsteadiness time scale is defined by the frequency of translational motion of the cylinder, whilst the ejection time scale is mainly determined by the rotational velocity of the cylinder. The afore mentioned characteristic parameters form the dimensionless numbers

$$Sx = \frac{x_u}{x_e}, \tag{7.1}$$

$$St = \frac{t_u}{t_e}. \tag{7.2}$$

Equations (7.1) and (7.2) can be utilized to determine a priori the type of separation in the flow. In figure 7-1 the suggested criteria to determine whether separation is fixed or moving are shown. The first step is to determine if the length scale at which ejection is occurring is smaller or greater than the characteristic length scale of unsteadiness. A separation structure will appear fixed if $Sx < 1$. In the rotor-oscillator arrangement this is equivalent to a flow where the translational motion of the cylinder is sufficiently small, such that independent of the motion frequency separation at the wall will appear fixed. If the translation of the cylinder is large, separation can be fixed or moving depending upon the time scales and nature of the flow, as indicated in the right branch of figure 7-1. Fixed separation will result if the ratio $St \leq O(1)$ and there exists a location on the boundary with zero-mean skin friction for all times, this is the case of the periodic flow and random flows considered in chapter 5. However, if there is not a point on the boundary with zero-mean skin friction, the type of separation can not be determined. An example of a flow that will satisfy $Sx > 1$, $St \leq O(1)$, and no zero-mean skin friction point on the boundary would be that resulting from a cylinder translating to a distance far from the origin in an infinitesimally small time; there is not evidence to ponder that separation is moving or is not occurring at all. Moving separation is guaranteed if $St \gg 1$. This is confirmed in chapter 6 for slow periodic flow and random-drift flow, in which the cylinder translation is slow compared to the ejection rate.

Taking the view that the flows studied clearly show either fixed or moving separation, utilizing the dimensionless numbers defined by (7.1) and (7.2) the results obtained can be

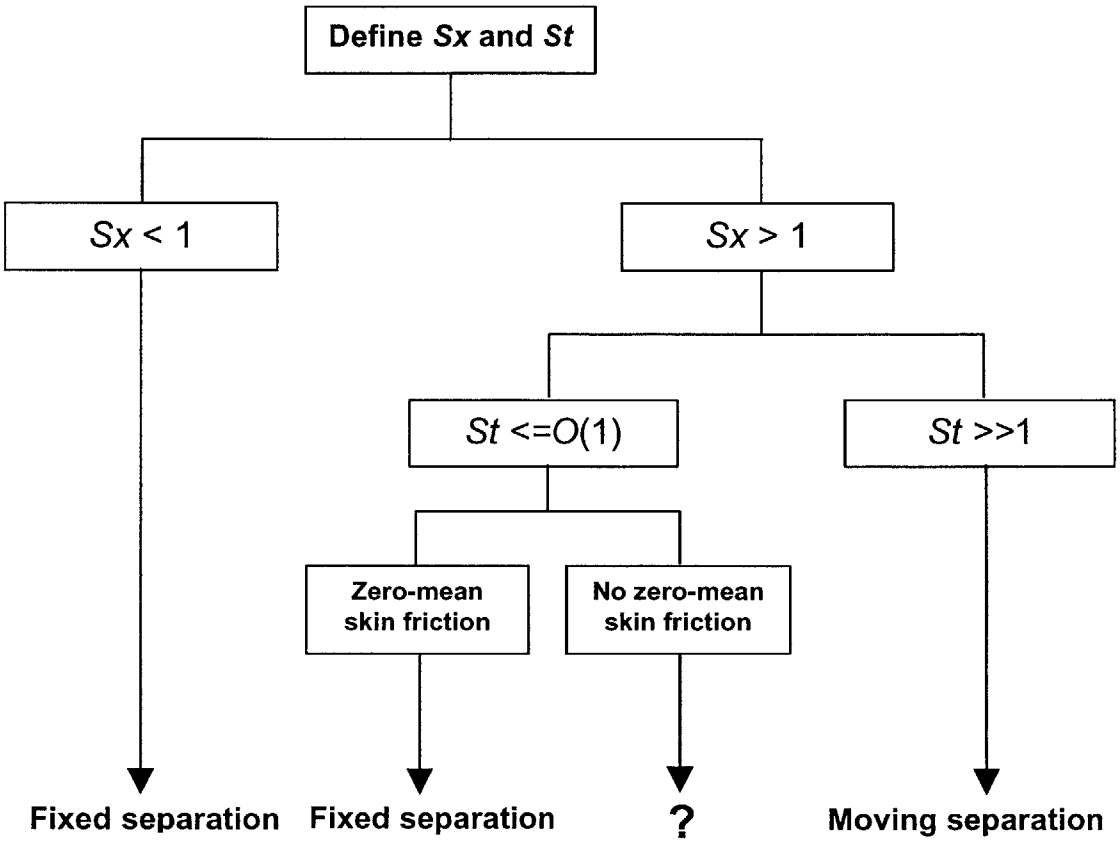

Figure 7-1: Chart indicating the type of separation according to the characteristic length and time scales of the flow.

Length scale	Time scale
$x_u = A$	$t_u = \frac{2\pi}{\alpha}$
$x_e = 3$ mm	$u_e = \left(\frac{x_e}{c}\right)^2 r\omega$, $t_e = \frac{x_e}{u_e} = \frac{c^2}{x_e^2\omega}$

Table 7.1: Unsteady and ejection length and time scales for experiments.

Fixed separation		Moving Separation	
Periodic flow		Slow periodic flow	
$A > x_e$	1-3 cm	$A > x_e$	3 cm
α	0.5- 2.5 rad/sec	α	0.01 rad/sec
$St = \frac{2\pi x_e^2 \omega}{d^2 \alpha}$	2-10	$St = \frac{2\pi x_e^2 \omega}{d^2 \alpha}$	540
Random flow		Random plus drift flow	
$B > r$	1-3 cm	$C > r$	6 cm
τ	1.5 sec	ξ	90 sec
$St = \frac{x_e^2 \tau \omega}{d^2}$	1.3	$St = \frac{x_e^2 \xi \omega}{d^2}$	78
for all exp. $\omega = 60$ rad/sec, $c = 2.5$ cm and $x_e = 3$ mm.			

Table 7.2: Summary of the flows studied according to separation type.

categorized. In table 7.1 the characteristic length and time scales are presented. Notice that the ejection length scale can not be easily quantified since there is ambiguity in defining the distance from the wall where the separation structure becomes the main stream. The experiments indicated that the ejection scale is of the order of millimeters, thus, from observation we estimate this value to on the order of 3 mm. The typical translation of the cylinder in the experiments is of the order of centimeters, hence, the type of separation is determined by the right branch of figure 7-1 since $S_x > 1$. The ejection time scale, t_e, is defined as the ratio of the ejection length scale, x_e, and ejection velocity, u_e. Because we are in a Stokes flow, a quadratic decay of the velocity as we move away from the cylinder is assumed.

Following the right branch of the chart in figure 7-1, the type of separation observed in the rotor-oscillator experiments is presented in table 7.2. In table 7.2, α is the frequency of oscillation of the periodic motion; τ, the time scale for the random motion without drift and ξ, the time scale for the linear drift of the random plus drift motion. Representing the relevant length scales are: A, the peak-to-peak amplitude of oscillation for the periodic motion; B the maximum peak-to-peak amplitude for the random motion and C the displacement of the random plus linear drift motion. Fixed separation and moving separation are distinguished by the magnitude of St.

The experimental and numerical results demonstrated the ability to predict the location of the separation point in unsteady flow and distinguish fixed from moving separation. However, errors originating in the dye visualization method and sensor technology for shear stress resulted in small discrepancies between experiments and theory. Inherent to dye visualization is the addition of mass to system and the finite width of the dye when taking measurements. By improving the visualization technique a greater resolution will be achieved; methods which are non-intrusive should be considered. Preliminary review of the visualization methods available indicate that the most promising option is utilizing Molecular Tagging Velocimetry (MTV) [12].

In regards to the shear stress measurements, it was not possible to directly confirm that the location of the zero skin friction point is not associated with the location of flow separation. The hot wires available allowed accurate measurements in steady and highly quasi-steady flows, such as the slow periodic flows. Nonetheless, the low heat transfer rate from sensor to fluid, due to the slow flow velocities, deterred shear measurements in flows with high Sr, such as the high frequency periodic and random flows. Fundamentally, the working principle of hot wires would require a sensing element order of magnitudes smaller than the ones utilized for the current work in order to measure shear stress in the periodic and random flows. Future efforts in measuring shear stress should explore alternative technologies that do not rely on heat transfer to the fluid as working principle for measurement. A possible alternative is the use of optical shear stress sensors [4].

Moving separation in unsteady flows with arbitrary flow dependence, such as the random plus drift flow, were not investigated in detail. The experimental observations and numerical simulations suggested that the Haller's criteria for moving separation qualitatively indicated the right trends. However, a degree of accuracy achieved in other flow types was not attained. In order to further validate Haller's ideas, it is necessary to further pursue experimentally and theoretically moving separation within flows of arbitrary time dependence.

The type of flows we have studied demonstrate that flow separation in an unsteady flow strongly depends on flow quantities on the wall weighted over time. As such, the instantaneous zero skin friction point by itself is clearly an erroneous measure of the location of unsteady flow separation. The experimental investigations verified the existence of fixed separation points and moving separation points in a viscous flow with different types of time dependence. More

specifically, it was demonstrated fixed separation occurs in flow fields at the location on the wall where the mean skin friction vanishes for all times. On the other hand, flow fields that do not possess a unique point with a zero-mean skin friction can admit a separation point that moves. Haller's criteria allowed concise and accurate investigation of flow separation. The theory promises a very robust approach to enlighten the mechanism and factors affecting separation in unsteady flow. By following Lagrangian ideas for separation, there exists tremendous potential for further theoretical tuning and fresh and creative experimental work.

Bibliography

[1] BATCHELOR, G. K. 1977 *An Introduction to Fluid Mechanics*, Cambridge University Press, New York.

[2] BLACKWELDER, R. F. 1981 Hot wire and hot film anemometers, In *Methods of Experimental Physics.* vol 18-A, pp 259 –314.

[3] FEARN, R. M., MULLIN, T. & CLIFFE, K. A. 1990 Nonlinear flow phenomena in a symmetric sudden-expansion. *J. Fluid Mech.* 211, 595 –608.

[4] GHARIB, M., MODARRESS, D., FOURGUETTE, D., & WILSON, D. 2002 Optical microsensors for fluid flow diagnostics, 40th AIAA Aerospace Sciences Meeting & Exhibit, Reno, Nevada.

[5] GUCKENHEIMER, J. & HOLMES, P. 1983 *Nonlinear Oscillations, Dynamical Systems, and Bifurcations of Vector Fields.* Appl. Math. Sci. vol.42, Springer-Verlag, New York.

[6] HACKBORN, W. W. 1987 Separation in interior Stokes flows driven by rotlets. Ph.D. thesis, University of Toronto.

[7] HACKBORN, W. W. 1990 Asymmetric Stokes flow between parallel planes due to a rotlet. *J. Fluid Mech.* 218, 531–546.

[8] HACKBORN, W. W., ULUCAKLI, M. E. & YUSTER, T. 1997 A theoretical and experimental study of hyperbolic and degenerate mixing regions in chaotic Stokes flow. *J. Fluid Mech.* 346, 23–48.

[9] HALLER, G. 2000 Finding finite-time invariant manifolds in two-dimensional velocity fields. *Chaos* 10, 99–108.

[10] HALLER, G. 2004 Exact theory on unsteady separation for two-dimensional flows. *J. Fluid. Mech.* 512, 257-311.

[11] LEKAKIS, I. 1996 Calibration and signal interpretation for single and multiple hot-wire/hot-film probes. *Meas. Sci. Technol.* 7, 1313-1333.

[12] LEMPERT, W. R & HARRIS, S. R. 2000 Flow tagging velocimetry using caged dye photo-activated fluorophores. *Meas. Sci. Technol.* 11, 1251–1258.

[13] LIGHTHILL, M. J. 1963 Boundary layer theory. In *Laminar Boundary Layers* (ed.L.Rosenhead). Dover.

[14] LIU, C. S. & WAN, Y. H. 1985 A simple exact solution of the Prandtl boundary layer equations containing a point of separation, *Arch. Rat. Mech. Anal.* 89, 177 –185.

[15] LUDWIG, G. R. 1964 An experimental investigation of laminar separation from a moving wall, AIAA Paper 64-6, AIAA, New York.

[16] MOORE, F. K. 1958 On the separation of unsteady boundary layer. In *Boundary-layer Research* (ed.H.G ¨ortler) pp.296–311. Springer.

[17] PRANDTL, L. 1904 Über Flüssigkeitsbewegung bei sehr kleiner Reibung. Verh.III, Int. Math. Kongr., Heidelberg pp.484 –491.

[18] ROTT, N. 1956 Unsteady viscous flows in the vicinity of a separation point. *Q. Appl. Maths* 13, 444 –451.

[19] SAHIN, M. , SANKAR, L. N., CHANDRASEKHARA, M. S., TUNG, C. 2000 Stall alleviation using a deformable leading edge concept. 38th AIAA Aerospace Sciences Meeting, AIAA 2000-0520, Reno, Nevada.

[20] SEARS,W. R. & TELLIONIS, D. P. 1971 Unsteady boundary layer separation. In *Recent Research on Unsteady Boundary Layers* (ed.E.Eichelbrenner), pp.404 –447.

[21] SEARS, W. R. &TELLIONIS, D. P. 1975 Boundary-layer separation in unsteady flow. *SIAM J. Appl. Maths* 28, 215 –235.

[22] SHARIFF, K., PULLIAM, T. H. & OTTINO, J. M. 1991 A dynamical systems analysis of kinematics in the time-periodic wake of a circular cylinder. *Lect. Appl. Math.* 28 ,613 –646.

[23] SWANSON, P. D. & OTIINO, J. M. 1990 A comparative computational and experimental study of chaotic mixing in viscous fluids. *J. Fluid Mech.* 213, 227–249.

[24] VAN DOMMELEN, L. L. 1981 Unsteady Boundary Layer Separation. Ph.D. thesis, Cornell University, Ithaca, NY.

[25] VAN DOMMELEN, L. L. & SHEN, S. F. 1982 The genesis of separation. In *Numerical and Physical Aspects of Aerodynamics Flow* (ed.T.Cebici) pp.283 –311. Long Beach, California.

[26] VIDAL, R. J. 1959 Research on rotating stall in axial-flow compressors, Part III – Experiments on laminar separation from a moving wall, Wright Air Development Center, TR-59-75, Wright-Patterson AFB, Dayton, Ohio.

[27] YUSTER, T. & HACKBORN, W. W. 1997 On invariant manifolds attached to oscillating boundaries of Stokes flows. *Chaos* 7 ,769 –776.